SOLUTIONS OF THE TWO-DIMENSIONAL, SUBSONIC FLOW ABOUT AN AIRFOIL

by

ALLAN LINWOOD CALDWELL

A THESIS

submitted to

OREGON STATE COLLEGE

in partial fulfillment of
the requirements for the
degree of

MASTER OF SCIENCE

June 1949

APPROVED:

Redacted for Privacy

Professor of Aeronautical Engineering

In Charge of Major

Redacted for Privacy

Head of Department of Mechanical Engineering

Redacted for Privacy

Chairman of School Graduate Committee

Redacted for Privacy

Dean of Graduate School

TABLE OF CONTENTS

ILLUSTRATIONS

TABLES

SYMBOLS

a	speed of sound
f	function
k	$\frac{M^2}{2(\beta + 1)}$
p	pressure
q	dynamic pressure = $1/2\ \rho\ v^2$
m	slope of lift curve
u, v	velocity component variables in x and y directions, respectively
u'	small perturbation velocity
w	resultant velocity
x, y	physical space coordinates
C	chord of airfoil
C_ℓ	lift coefficient = $\frac{\text{lift}}{qS}$
C_n	normal force coefficient = $\frac{\text{normal force}}{qS}$
C_p	pressure coefficient = $\frac{p - p_\infty}{q_\infty}$
K	constant
M	Mach number = $\frac{U}{a_\infty}$
P	$C_{p_\ell} - C_{p_u}$
S	area
U	free stream velocity in x direction at ∞
W	velocity computed on incompressible flow assumption
α	angle of attack
β	$\sqrt{1 - M^2}$

SYMBOLS (Cont'd)

γ	ratio of specific heats
Δ	small change
η	$(C_{\ell} - C_{\ell_b})$
θ	polar coordinate variable
λ	distortion factor $= \frac{U^2}{4a_o^2}$
ρ	mass density
ω	transformation variable $= (\sqrt{1 - M^2})(\ln w)$
ϕ	velocity potential
Ψ	stream function
Ω	transformation variable $= \ln W$

Subscripts

a	additional, as due to angle of attack only
b	base profile; dependent upon camber-line shape only
c	sonic
f	local
i	incompressible
ℓ	lower surface of airfoil
m	compressible
o	stagnation conditions
u	upper surface of airfoil
∞	free stream conditions
1, 2	particular values

SOLUTIONS OF THE TWO-DIMENSIONAL, SUBSONIC FLOW ABOUT AN AIRFOIL

I. INTRODUCTION

A. General.

For many years the theory of aerodynamics has been able to predict useful results by assuming, among other things, that air is incompressible. Although this assumption was obviously wrong, the resulting theory allowed accurate calculations of pressure distributions and lift forces on airfoil sections. At air speeds of less than 300 miles per hour, this basic assumption is very nearly true. The development of high-speed airplanes in the last ten years, however, has necessitated extensive research into the effects of the compressibility of air upon the flows about aerodynamic shapes used in aircraft for lift, propulsion, and control. These effects are quite pronounced as the velocity of the free stream about the shape approaches the velocity of sound. The theoretical treatment of the flow then is much more difficult, and even at the present time, no success has been attained comparable to that of the theory of incompressible flow. The results of these difficulties have meant large expenditures for high-speed wind tunnel construction and testing, and elaborate and expensive flight tests. The need for good analytical methods that can be applied to practical aerodynamic shapes is acute.

At the present time, the majority of our airplanes are flying at speeds ranging from 1/2 U_c to U_c, or at subsonic speeds. This subsonic range of speeds is not only important from the present practical standpoint, but it also represents a difficult point in the theory. The basic problem is to determine the pressure or velocity distribution over an airfoil of arbitrary shape, taking into account the compressibility of the air. The condition of two-dimensional flow is equivalent to considering a wing section of infinite span in a flow which is the same for every plane perpendicular to the wing. This, of course, does not accurately represent actual conditions, but it does allow consideration of the lift forces on the airfoil. Two-dimensional subsonic flow theory does not allow consideration of drag forces.

In the past five years the aerodynamicist who has been faced with this problem of calculating the pressure distribution over an airfoil, has encountered a wealth of theoretical work on the subject. Many have been appalled at the large amount of mathematics employed in the discussions, and the obvious lack of practical methods which could be applied in engineering work. Briefly, the theoretical difficulties stem from the fact that the differential equations describing the flow are non-linear. As yet a general method for the treatment of non-linear partial differential equations does not exist. However, two methods are generally used to find solutions to these equations of motion:

1. To approximate the exact non-linear equations by linear differential equations.
2. To try to find a transformation of variables that transforms the exact non-linear equations into exact linear equations.

B. Object of Investigation.

The object of this paper is to determine the pressure distribution around a given airfoil in two-dimensional, subsonic flow by available methods, and to attempt to evaluate these methods by correlating their results with experimental data that has been published on the subject. It is hoped that the investigation will provide some ideas for future research in this important problem.

II. AIRFOIL SELECTION

The first step in the problem is the selection of the airfoil. For the purposes of the investigation, an airfoil is needed with extensive compressible and incompressible experimental data available. In order to simplify the work as much as possible, it would also be desirable to have an airfoil with theoretical, incompressible calculations either completed or in such a form that could be easily calculated for the desired conditions.

Fortunately, the National Advisory Committee for Aeronautics' 4412 airfoil (5, p.320) satisfies these conditions. Very complete experimental work has been done with this airfoil at high speeds in

an attempt to investigate the effects of compressibility. Since, in the theory developed later, compressible flows are related to the corresponding incompressible flows, it is important to have reliable calculations for the incompressible flow. In a recent method of calculating pressure distributions (1, p.21), theoretical data are presented for the NACA 4412 airfoil, and can be used to calculate the incompressible flow easily. From other considerations, however, the NACA 4412 airfoil is not really a "modern" airfoil, in that it does not have low drag characteristics. It will probably not appear on any future airplanes. Physically speaking, it has a maximum thickness of 12 per cent (of the chord), which occurs at 40 per cent of the chord behind the leading edge. Its thickness of 12 per cent makes it a relatively thin airfoil, which is a necessity for high-speed considerations. Because of the favorable factors mentioned, the NACA 4412 airfoil was chosen for the investigation. Its drag characteristics will be overlooked since drag is not being considered in the investigation. It is believed that the undesirable characteristics of the airfoil will in no way alter the usefulness of the investigation. The airfoil and its coordinates appear in Figure 1.

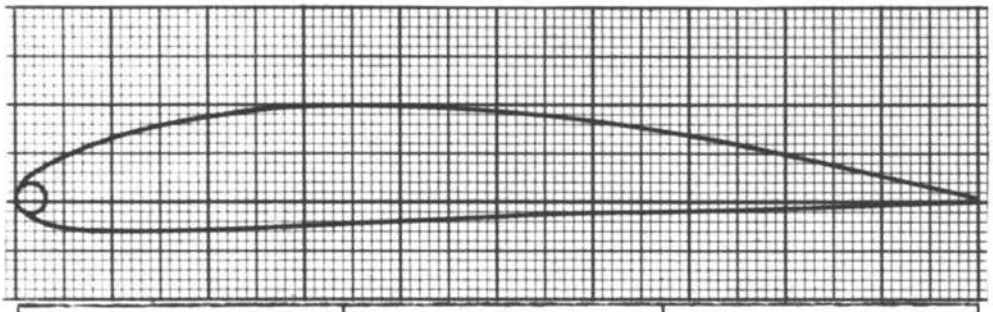

Station	Upper	Lower
0	---	0
1.25	2.44	-1.43
2.50	3.39	-1.95
5.00	4.73	-2.49
7.50	5.76	-2.74
10.00	6.59	-2.86
15.00	7.89	-2.88
20.00	8.80	-2.74
25.00	9.41	-2.50
30.00	9.76	-2.26
40.00	9.80	-1.80
50.00	9.19	-1.40
60.00	8.14	-1.00
70.00	6.69	-0.65
80.00	4.89	-0.39
90.00	2.71	-0.22
95.00	1.47	-0.16
100.00	(0.13)	(-0.13)
100.00	---	0
L.E. Radius = 1.58 Slope of Radius Through End of Chord : 4/20		

Figure 1.

NACA 4412 Airfoil Section (6, p.320).

III. THE EQUATIONS OF FLOW

A. Basic Assumptions.

In order to derive the equations that describe the flow of a compressible fluid in two dimensions, it is first necessary to state the basic assumptions upon which the derivation will depend. It will be assumed that the following exists:

1. Steady flow (independent of time)
2. Reversible adiabatic flow (frictionless and isentropic)
3. A perfect, compressible gas or fluid that makes up the flow
4. An irrotational flow (or potential flow)

B. Equation of Continuity.

The equation of continuity expresses the fact that the mass flow in the fluid is a constant. In other words, the amount of fluid entering a small element is equal to the amount of fluid leaving that element in unit time. Figure 2 shows a small element in the flow.

The mass of fluid entering the element per unit time is $\rho u\, \Delta y + \rho v\, \Delta x$. At the faces $(x + \Delta x)$ and $(y + \Delta y)$, the change in ρu may be expressed by an expansion in Taylor's series. Thus, equating the amount of fluid entering and the amount leaving, we have,

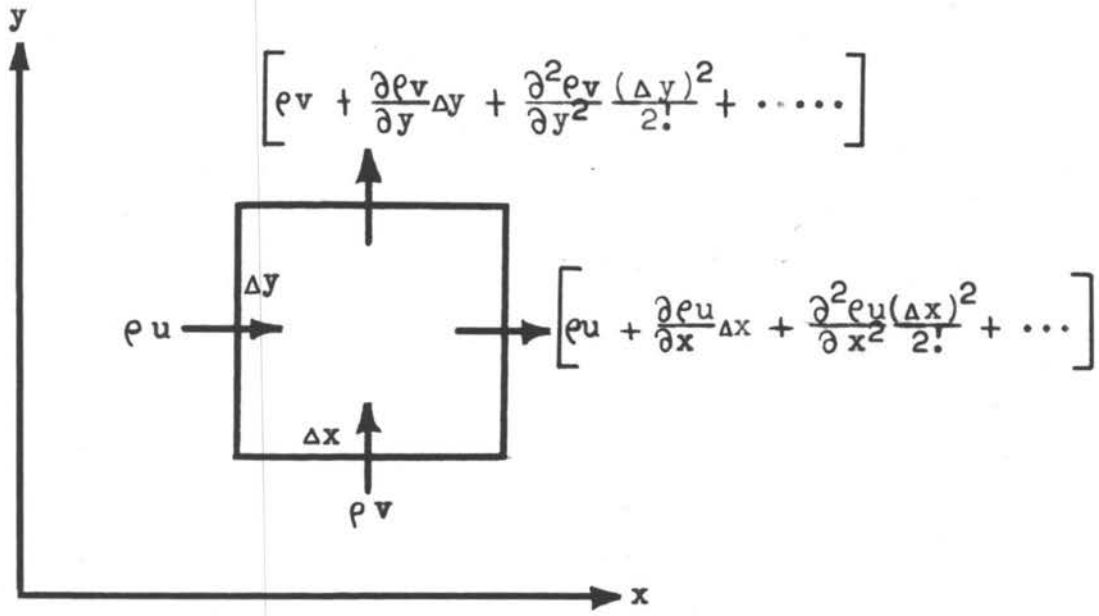

Figure 2.

Small Element in Continuous Flow.

$$\rho u \Delta y + \rho v \Delta x = \left[\rho u + \frac{\partial \rho u}{\partial x} \Delta x + \frac{\partial^2 \rho u}{\partial x^2} \frac{(\Delta x)^2}{2!} + \ldots . \right] \Delta y$$

$$+ \left[\rho v + \frac{\partial \rho v}{\partial y} \Delta y + \frac{\partial^2 \rho v}{\partial y^2} \frac{(\Delta y)^2}{2!} + \ldots . \right] \Delta x.$$

Simplifying the above expression leads to the equation,

$$\left[\frac{\partial \rho u}{\partial x} \Delta x \Delta y + \frac{\partial^2 \rho u}{\partial x^2} \frac{(\Delta x)^2 \Delta y}{2!} + \ldots . \right]$$

$$+ \left[\frac{\partial \rho v}{\partial y} \Delta y \Delta x + \frac{\partial^2 \rho v}{\partial y^2} \frac{(\Delta y)^2 \Delta x}{2!} + \ldots . \right] = 0.$$

Now, dividing by $(\Delta x \Delta y)$, and taking the limit as Δx and Δy approach zero, gives the result,

$$\frac{\partial \rho u}{\partial x} + \frac{\partial \rho v}{\partial y} = 0. \qquad (1)$$

This is the equation of continuity. Because the fluid is compressible, ρ is a function of x and y and must remain as part of the product ρu or ρv, unless the form for the differentiation of a product is used.

C. The Equation of Motion.

The equations of motion represent Newton's law. This law states that the sum of the forces acting on any element in a steady flow is equal to the product of the mass and the acceleration. In Figure 3 is shown a small element in the flow.

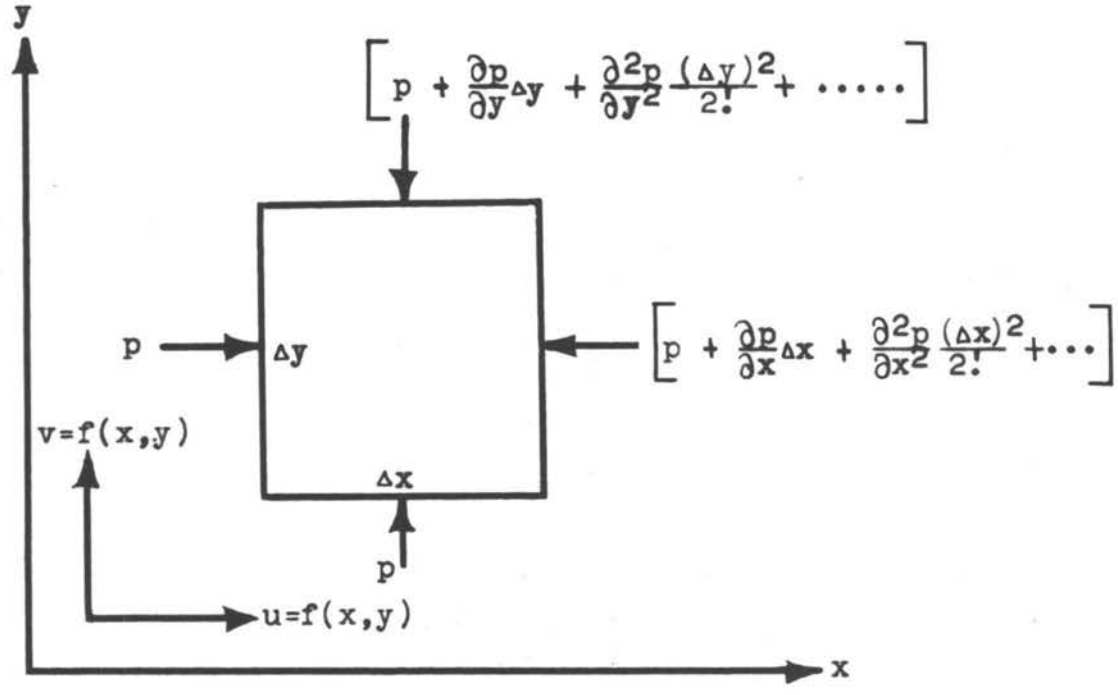

Figure 3.

Small Element Showing Pressures Acting.

The pressure on the face $x + \Delta x$ is expanded in a Taylor's series. Equating the sum of the forces and the product of the mass and acceleration in the x direction, we have,

$$p\Delta y - \left[p + \frac{\partial p}{\partial x}\Delta x + \frac{\partial^2 p}{\partial x^2}\frac{(\Delta x)^2}{\partial !} + \ldots . \right] \Delta y = \rho \Delta y \Delta x \left(\frac{du}{dt}\right).$$

By simplifying the above expression and expressing $\left(\frac{du}{dt}\right)$ in partial derivatives, we obtain,

$$- \left[\frac{\partial p}{\partial x}\Delta x \Delta y + \frac{\partial^2 p}{\partial x^2}\frac{(\Delta x)^2 \Delta y}{\partial !} + \ldots . \right] = \rho \Delta y \Delta x \left[\frac{\partial u}{\partial x}\frac{dx}{dt} + \frac{\partial u}{\partial y}\frac{dy}{dt} \right].$$

But, by definition, $\left(\frac{dx}{dt}\right) = u$, and $\left(\frac{dy}{dt}\right) = v$, so,

$$- \left[\frac{\partial p}{\partial x}\Delta x \Delta y + \frac{\partial^2 p}{\partial x^2}\frac{(\Delta x)^2 \Delta y}{\partial !} + \ldots . \right] = \rho \Delta y \Delta x \left[u\frac{\partial u}{\partial x} + v\frac{\partial u}{\partial y} \right].$$

Now, dividing by $(\Delta x, \Delta y)$, and taking the limit as Δx and Δy approach zero, we obtain,

$$- \frac{\partial p}{\partial x} = \rho \left[u\frac{\partial u}{\partial x} + v\frac{\partial u}{\partial y} \right].$$

Or,

$$u\frac{\partial u}{\partial x} + v\frac{\partial u}{\partial y} = -\frac{1}{\rho}\frac{\partial p}{\partial x}. \qquad (2)$$

The same procedure may be followed in the y direction, with the results,

$$u\frac{\partial v}{\partial x} + v\frac{\partial v}{\partial y} = -\frac{1}{\rho}\frac{\partial p}{\partial y}. \qquad (3)$$

Equations (2) and (3) express Newton's law for a compressible fluid in a steady flow.

D. Summary.

The equation of continuity and the equations of motion, that have just been derived, form the basis for the equations of flow. In order to obtain a more practical form, consider the second assumption in part A, that is, that the flow is reversible adiabatic. For this type of process, the following equation holds true,

$$p = K \rho^{\gamma} . \tag{4}$$

Equation (4) will be used to eliminate ρ from the equation of continuity. Taking the logarithm of each side of equation (4) and differentiating, say, with respect to y, gives the result,

$$\frac{1}{\rho} \frac{\partial p}{\partial y} = \frac{\gamma}{\rho} \frac{\partial \rho}{\partial y} .$$

But it is shown in aerodynamics (6, p.21) that $a^2 = \gamma \frac{p}{\rho}$. Thus, this substituted into the above equation gives,

$$\frac{\partial p}{\partial y} = a^2 \frac{\partial \rho}{\partial y} . \tag{5}$$

Similarly,

$$\frac{\partial p}{\partial x} = a^2 \frac{\partial \rho}{\partial x} . \tag{6}$$

If the rule for the differentiation of a product is applied to equation (1), the following results,

$$\rho \frac{\partial u}{\partial x} + u \frac{\partial \rho}{\partial x} + \rho \frac{\partial v}{\partial y} + v \frac{\partial \rho}{\partial y} = 0. \tag{7}$$

In order to apply equations (5) and (6) to equation (7), multiply (7) by $(\frac{a^2}{\rho})$.

$$a^2 \frac{\partial u}{\partial x} + \frac{ua^2}{\rho} \frac{\partial \rho}{\partial x} + a^2 \frac{\partial v}{\partial y} + \frac{va^2}{\rho} \frac{\partial \rho}{\partial y} = 0. \qquad (8)$$

Now substitute (5) and (6) into (8). This gives,

$$a^2 \frac{\partial u}{\partial x} + \frac{u}{\rho} \frac{\partial p}{\partial x} + a^2 \frac{\partial v}{\partial y} + \frac{v}{\rho} \frac{\partial p}{\partial y} = 0. \qquad (9)$$

The second and fourth terms above are seen to be the same as the right hand sides of equations (2) and (3) except for sign and the velocity factors u and v. Substituting equations (2) and (3) into equation (9) results in,

$$a^2 \frac{\partial u}{\partial x} - u^2 \frac{\partial u}{\partial x} - uv \frac{\partial u}{\partial y} + a^2 \frac{\partial v}{\partial y} - uv \frac{\partial v}{\partial x} - v^2 \frac{\partial v}{\partial y} = 0.$$

Or,

$$(a^2 - u^2) \frac{\partial u}{\partial x} + (a^2 - v^2) \frac{\partial v}{\partial y} - uv \left(\frac{\partial u}{\partial y} + \frac{\partial v}{\partial x}\right) = 0. \qquad (10)$$

Equation (10) is the combination of the equations of motion, the continuity equation, and the assumption of reversible adiabatic flow. If the flow is irrotational, the velocity components may be given in terms of a velocity potential, ϕ, as follows (10, p.94),

$$u = \frac{\partial \phi}{\partial x} \quad \text{and} \quad v = \frac{\partial \phi}{\partial y}. \qquad (11)$$

The equations (11), when substituted into (10), give,

$$\left[a^2 - \left(\frac{\partial \phi}{\partial x}\right)^2\right] \frac{\partial^2 \phi}{\partial x^2} + \left[a^2 - \left(\frac{\partial \phi}{\partial y}\right)^2\right] \frac{\partial^2 \phi}{\partial y^2} - 2\left(\frac{\partial \phi}{\partial x}\right)\left(\frac{\partial \phi}{\partial y}\right)\left[\frac{\partial^2 \phi}{\partial x \partial y}\right] . \qquad (12)$$

Equation (12) represents the end result of the equations of flow and is the equation that must be solved for the compressible, reversible adiabatic, irrotational, steady flow of a perfect fluid. The problem is then to find a solution of the non-linear equation (12) to fit arbitrary boundary conditions. Inability to obtain a general solution to this equation is responsible for most of the problems in the present theory of compressible aerodynamics at subsonic speeds. At the present time there are two methods of solution that are of practical importance to the engineer; the Prandtl-Glauert Approximation, and the Karman-Tsien Approximation. These will be discussed in the next section.

IV. APPROXIMATE METHODS OF SOLUTION

As mentioned in the introduction, the approximate methods of solution are based on two methods. The first of these methods is to linearize the equations of motion by some approximation, and the second method is to find some transformation that will reduce the non-linear equations to linear equations without the use of any approximation. In this investigation, an application of each method will be covered.

A. The Prandtl-Glauert Method.

One of the first and best known methods for calculating the compressibility effects for an airfoil was due to Prandtl and Glauert (4, p.235). This method is of the first type; that is, it

makes use of an approximation which linearizes the equations of motion. This approximation is generally referred to as the small perturbation method. The reason for this will become apparent. In order to develop this method, it will be convenient to rewrite equation (12) by dividing through by a^2, and expressing it in the following form:

$$(1 - \frac{u^2}{a^2}) \frac{\partial^2 \phi}{\partial x^2} + (1 - \frac{v^2}{a^2}) \frac{\partial^2 \phi}{\partial y^2} - \frac{2uv}{a^2} \frac{\partial^2 \phi}{\partial x \partial y} = 0. \qquad (13)$$

It will be assumed that our airfoil under consideration is thin and that the airstream coming from infinity at the velocity, U, is increased over the airfoil so that the x component is U + u', where u' is a small perturbation velocity. In the free stream at infinity, v = 0, while around the airfoil v = v. It will now be assumed that,

1. $\frac{u'^2}{U^2}$, $\frac{v^2}{U^2}$ are negligible compared to 1.

2. $\frac{(\gamma - 1)(M^2)(u')}{U^2}$ is negligibly small.

3. $\frac{2u'}{U}$, $\frac{M^2 v^2}{U^2}$ are negligible compared to 1.

The importance of the second assumption will be seen presently, for, if Bernoulli's equation for a compressible, reversible, adiabatic flow is written, we have,

$$a^2 + (\frac{\gamma - 1}{2}) w^2 = a_\infty^2 + (\frac{\gamma - 1}{2}) w_\infty^2. \qquad (14)$$

But, $w^2 = u^2 + v^2 = (U + u')^2 + v^2$, and $w_\infty^2 = U^2$. If this is substituted into equation (14), and the equation is transposed, the following results,

$$a^2 = a_\infty^2 + \left(\frac{\gamma - 1}{2}\right)\left[-2Uu' - u'^2 - v^2\right] . \qquad (15)$$

Dividing through by a^2 gives the expression,

$$\frac{a^2}{a_\infty^2} = 1 + \frac{\gamma - 1}{2}\left[\frac{-2Uu' - u'^2 - v^2}{a_\infty^2}\right] . \qquad (16)$$

Or, since $a_\infty^2 = \frac{U^2}{M^2}$,

$$\frac{a^2}{a_\infty^2} = 1 + \left(\frac{\gamma - 1}{2}\right)\left[\frac{M^2(-2Uu' - u'^2 - v^2)}{U^2}\right] . \qquad (17)$$

By applying the first assumption made, it is found that equation (17) reduces to,

$$\frac{a^2}{a_\infty^2} = 1 - \frac{(\gamma - 1)(M^2)(u')}{U} . \qquad (18)$$

The reason for the second assumption is now apparent, for because of it, equation (18) reduces to $\frac{a^2}{a_\infty^2} = 1$. From this, it is now evident that,

$$\frac{U^2}{a^2} = \frac{U^2}{a_\infty^2} \cdot \frac{a_\infty^2}{a^2} = M^2$$

Approximately (19)

$$\frac{u^2}{a^2} = \frac{u^2}{U^2} \cdot \frac{U^2}{a^2} = \left(1 + \frac{2u'}{U}\right)M^2 .$$

The use of assumption (3) in the second equation of (19) reduces it to,

$$\frac{u^2}{a^2} = (1 + \frac{2u'}{U})\, M^2 \cong M^2. \tag{20}$$

Also, $\frac{v^2}{a^2} = \frac{v^2 M^2}{U^2}$ from equation (19). But this is negligibly small compared to one by assumption (3) and can be neglected. The term $2(\frac{uv}{a^2})(\frac{\partial^2 \phi}{\partial x \partial y})$ is equal to,

$$2(\frac{uv}{a^2})(\frac{\partial^2 \phi}{\partial x \partial y}) = \frac{2M^2 v}{U} \frac{\partial^2 \phi}{\partial x \partial y} + \frac{2M^2 u' v}{U^2} \frac{\partial^2 \phi}{\partial x \partial y}. \tag{21}$$

Since u' and v are of approximately the same magnitude, the terms on the right hand side of equation (21) are negligible under assumptions (1) and (3).

If the three results of the assumptions above are applied to the fundamental equation (13), the following linear equation results,

$$(1 - M^2) \frac{\partial^2 \phi}{\partial x^2} + \frac{\partial^2 \phi}{\partial y^2} = 0. \tag{22}$$

Equation (22) is the basic linearized equation of flow. In order to solve this equation, Glauert and Prandtl introduced a new set of variables. Thus, let

$$y' = y$$

$$x' = \frac{x}{\sqrt{1 - M^2}}. \tag{23}$$

Then, forming the new derivatives,

$$\frac{\partial \phi}{\partial x} = \frac{\partial \phi}{\partial x'} \frac{dx'}{dx} = \frac{1}{\sqrt{1 - M^2}} \frac{\partial \phi}{\partial x'}$$

$$\frac{\partial^2 \phi}{\partial x^2} = \frac{\partial \frac{\partial \phi}{\partial x}}{\partial x'} \frac{dx'}{dx} = \frac{1}{1 - M^2} \frac{\partial^2 \phi}{\partial x'^2} \tag{24}$$

$$\frac{\partial \phi}{\partial y} = \frac{\partial \phi}{\partial y'} \frac{dy'}{dy} = \frac{\partial \phi}{\partial y'} .$$

$$\frac{\partial^2 \phi}{\partial y^2} = \frac{\partial \frac{\partial \phi}{\partial y}}{\partial y'} \frac{dy'}{dy} = \frac{\partial^2 \phi}{\partial y'^2} .$$

Substituting equation (24) into equation (22) gives,

$$\frac{\partial^2 \phi}{\partial x'^2} + \frac{\partial^2 \phi}{\partial y'^2} = 0. \tag{25}$$

This is Laplace's equation and represents the equation for an incompressible flow. If the solution to this equation is found at (x_1', y_1') in the incompressible flow, the value of ϕ will be, say, ϕ_1. Then at the point (x_1, y_1), defined by equation (23), the velocity potential will still be ϕ_1. Thus the effect of the compressibility may be thought of as acting in either of two ways. For a given flow, the compressibility has the effect of decreasing the chord of the airfoil in the incompressible flow by the factor, $\sqrt{1 - M^2}$. Or, if the compressible and incompressible flows are being compared about the same airfoil, the compressibility has the

effect of increasing the pressure coefficient of the incompressible flow by the factor $\frac{1}{\sqrt{1 - M^2}}$. Thus,

$$C_{p_m} = \frac{C_{p_i}}{\sqrt{1 - M^2}} . \tag{26}$$

However, the lift coefficient may be expressed in terms of the pressure coefficient (7, p.140).

$$C_{l_m} = \frac{1}{C}\int_0^C (C_{p_u} - C_{p_l})_m \, dx = \frac{\frac{1}{C}\int_0^C (C_{p_u} - C_{p_l})_i \, dx}{\sqrt{1 - M^2}} . \tag{27}$$

Or,

$$C_{l_m} = \frac{C_{l_i}}{\sqrt{1 - M^2}} . \tag{28}$$

This is the final result of the Prandtl-Glauert approximation. Due to the assumptions made, it is obvious that the region of accuracy of equation (28) is limited to the cases of low Mach numbers, small angles of attack, and thin airfoils.

B. The Karman-Tsien Approximation.

The Karman-Tsien approximation is an application of the so-called hodograph method, which utilizes the fundamental idea of converting the non-linear partial differential equations of flow into linear equations of flow by a transformation of coordinates. Basically, this transformation of coordinates amounts to

describing the flow in a system in which the velocities, u and v become the independent variables in place of x and y. The fact that the non-linear equations of flow are transformed into linear equations might at first appear to be the answer to all the problems in compressible flow. This, however, is not the case, for the hodograph has one distinct drawback. This is in the matter of boundary conditions. The boundary conditions for the problem are specified in terms of the geometric shape of the airfoil, and it is generally difficult to find a solution in the hodograph plane that will satisfy arbitrary boundary conditions in the physical plane. In order to get a better picture of the situation, consider Figure 4, which shows a comparison of the physical and hodograph planes.

The streamline a-b-c-d-e along the upper surface of the airfoil in the physical plane is represented by the streamline a'-b'-c'-d'-e' in the hodograph plane. The points b and d are stagnation points. Thus, it is seen that the flow about the airfoil in the physical plane may be represented in the hodograph plane.

The method of the hodograph was first developed by Molenbreck in 1898 (6, p.163), and by Chaplygin in 1902 (2, p.4). This work went practically unnoticed until the early nineteen-thirties, and Chaplygin's paper was not translated until 1944. Since the complete derivation of the hodograph transformation and the Karman-Tsien approximation is extremely long and difficult,

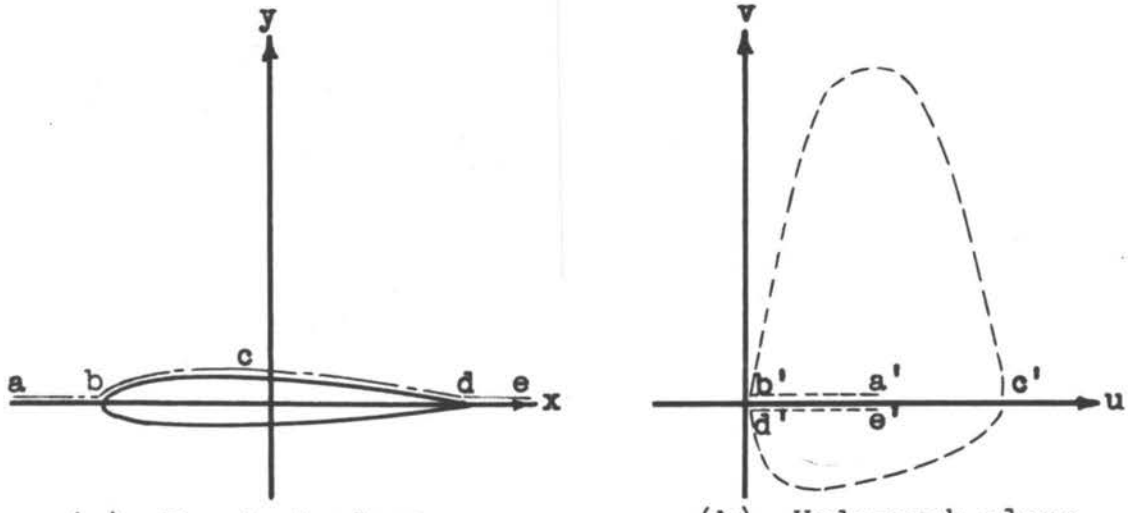

(a). Physical plane. (b). Hodograph plane.

Figure 4.

Streamline in the Physical and Hodograph Planes (6, p.14).

only the fundamental principles of the method will be presented here. The only two complete derivations of the hodograph method and the Karman-Tsien approximation as applied to compressible aerodynamics, that are known by the author to be available at the present time, are the original paper by Theodore von Karman (12, p.337), and a recent text on aerodynamics (6, p.163). For a detailed account of the procedure, either of these references is good.

Basically, the procedure has six steps. The object of this section will be to present an outline of the procedure and the basic equations that result from it.

The first step is the derivation of the equations of flow in the physical plane in terms of the stream function, Ψ, and the velocity potential, ϕ, with w and Θ as the dependent variables. This is done with the same basic assumptions as in Part III of this paper. The results of this are (6, p.169),

$$\frac{\rho}{\rho_o} w \frac{\partial \Theta}{\partial \Psi} + (1 - M^2) \frac{\partial w}{\partial \phi} = 0$$

$$w \frac{\partial \Theta}{\partial \phi} - \frac{\rho}{\rho_o} \frac{\partial w}{\partial \Psi} = 0. \qquad (29)$$

The second step in the process is to transform the equations (29) into the hodograph plane. In (29), $\Theta = f(\phi, \Psi)$, and $w = f(\Theta, \Psi)$. In order to effect the hodograph transformation, equations must be found that express $\phi = f(w, \Theta)$ and $\Psi = f(w, \Theta)$. This is done by writing the total differentials for ϕ, Ψ, and then

solving for dw and $d\theta$ by determinants, with the results,

$$\frac{\rho}{\rho_o} w \frac{\partial \phi}{\partial w} + (1 - M^2) \frac{\partial \psi}{\partial \theta} = 0$$

$$w \frac{\partial \psi}{\partial w} - \frac{\rho}{\rho_o} \frac{\partial \phi}{\partial \theta} = 0. \qquad (30)$$

Equation (30) represents the equation of flow in the hodograph plane in the polar coordinates, w and θ. The above equations are linear since the coefficients of the derivatives are functions of the independent variables only.

If incompressible flow in the hodograph plane is considered, $\frac{\rho}{\rho_o} = 1$ and equations (30) will reduce to the Cauchy-Reimann differential equations if $\Omega = \log W$ and θ are used as independent variables. Similarly, for compressible flow, if a variable ω is given as $d\omega = \sqrt{1 - M^2}\, \frac{dw}{w}$, equations (30) reduce to the symmetrical form,

$$\frac{\partial \phi}{\partial \omega} = - \frac{\rho_o}{\rho} \sqrt{1 - M^2}\, \frac{\partial \psi}{\partial \theta}$$

$$\frac{\partial \phi}{\partial \theta} = + \frac{\rho_o}{\rho} \sqrt{1 - M^2}\, \frac{\partial \psi}{\partial \omega} . \qquad (31)$$

It is seen from the above equations that if the quantity $\frac{\rho_o}{\rho} \sqrt{1 - M^2}$ could be put equal to unity, equations (31) would reduce to the Cauchy-Reimann differential equations. This is an important point in the procedure. From the isentropic relation of flow (6, p.174), we have,

$$\frac{\rho_o}{\rho}\sqrt{1 - M^2} = 1 + \left(\frac{\gamma - 1}{2}\right)^{\frac{1}{\gamma-1}} \sqrt{1 - M^2} \quad . \tag{32}$$

Now, if γ had the value of $\gamma = -1$, equation (32) would be equal to unity, the desired result. Actually, no gas exists with a ratio of specific heats equal to -1, but Chaplygin considered a $\gamma = -1$ as an approximation to the isentropic relation for the gas. Chaplygin used the line tangent to the $p = K\rho^{\gamma}$ curve at the point p_o, ρ_o, which represented stagnation conditions. It is interesting to note that incompressible flow has the relation, $\rho_o = K$. The Karman-Tsien approximation uses the tangent to the curve at p_∞, ρ_∞, or at free stream conditions. This covers a wider range of applicability. Figure 5 illustrates these approximations.

To represent this tangent at p_∞, ρ_∞, Karman and Tsien use the form,

$$p - p_\infty = p_\infty^2 a_\infty^2 \left(\frac{1}{\rho_\infty^2} - \frac{1}{\rho^2}\right) . \tag{33}$$

Let us now consider the effects of the approximation. The compressible Bernoulli equation with $\gamma = -1$ becomes,

$$w^2 - a_\infty^2 = w^2 - a^2 . \tag{34}$$

The hodograph equations (31) become,

$$\begin{aligned} \frac{\partial \phi}{\partial \omega} &= -\frac{\partial \psi}{\partial \theta} \\ \frac{\partial \phi}{\partial \theta} &= \frac{\partial \psi}{\partial \omega} . \end{aligned} \tag{35}$$

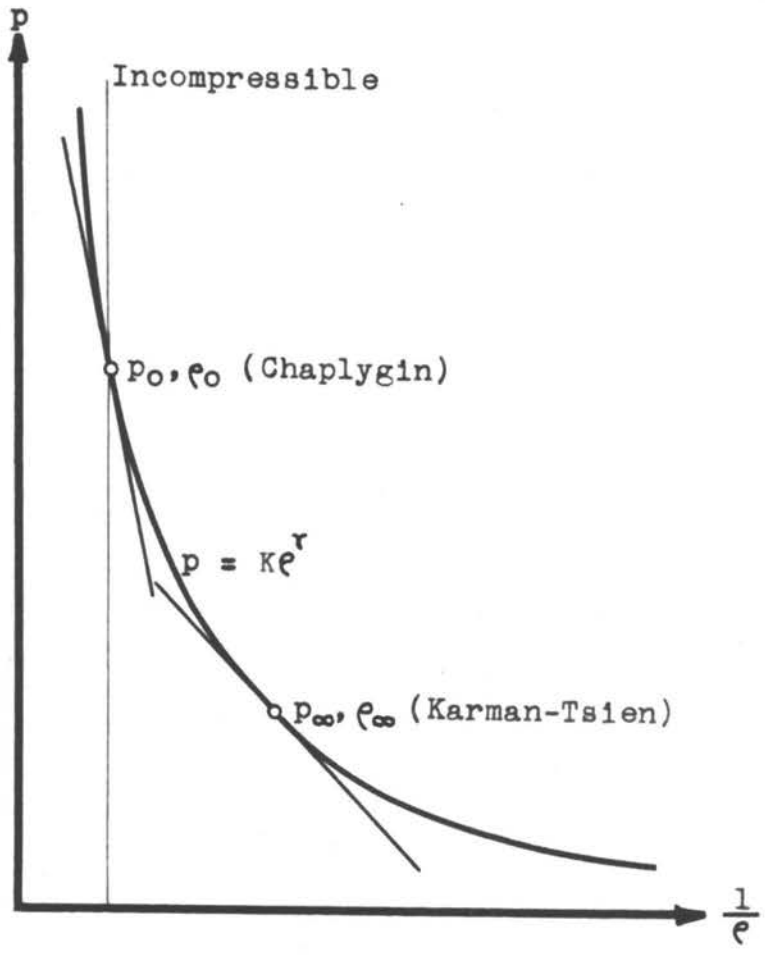

Figure 5.

Approximations of Chaplygin and Karman-Tsien (12, p. 345).

The corresponding incompressible hodograph equations follow from (30) with $\frac{\rho}{\rho_o} = 1$, and will reduce to the Cauchy-Reimann differential equations with $\Omega = \log W$. Therefore, the relationship between the incompressible velocity, W, and the compressible velocity, w, comes from the relation of Ω and ω such that both will satisfy the Cauchy-Reimann equations if,

$$\frac{dW}{W} = \sqrt{1 - M^2}\,\frac{dw}{w}\,. \tag{36}$$

Equation (36) is integrated with the help of equation (34) and the following results between incompressible and compressible velocities are obtained:

$$w = \frac{4a_o^2\, W}{4a_o^2 - W^2}\,. \tag{37}$$

Also, from equation (34) and Chaplygin's approximation, it is shown that,

$$\frac{\rho_o}{\rho} = \frac{4a_o^2 + W^2}{4a_o^2 - W^2}\,. \tag{38}$$

Equations (37) and (38) give the complete set of relations between an incompressible and a compressible flow. However, the problem is not completely finished for it must be shown that the incompressible and compressible flow as described by equations (37) and (38) apply to the same boundary. A detailed analysis of this question (6, p.179) reveals that there is a slight distortion in profile which is dependent upon the shape of the boundary and on the factor,

$$\lambda = \frac{W_\infty^2}{4a_o^2} . \tag{39}$$

λ is seen to become greater with increased Mach number, but even at speeds close to Mach = 1, the distortion factor is small. In most cases it is completely neglected.

In order to apply equations (37) and (38), we have, from the definition of pressure coefficient, and equation (33),

$$C_{p_m} = \frac{p - p_\infty}{q_\infty} = 2 \frac{a_\infty^2}{W_\infty^2} \left(1 - \frac{\rho_\infty}{\rho}\right). \tag{40}$$

Also, the Bernoulli equation for incompressible flow gives,

$$C_{p_i} = 1 - \frac{W^2}{U^2} . \tag{41}$$

By use of equations (37), (38), and the fact that,

$$\frac{\rho_\infty}{\rho} = \frac{\rho_\infty}{\rho_o} \cdot \frac{\rho_o}{\rho} = \frac{4a_o^2 - U^2}{4a_o^2 + U^2} \cdot \frac{4a_o^2 + W^2}{4a_o^2 - W^2} = \left[\frac{1-\lambda}{1+\lambda}\right] \frac{(1+\lambda)\left(\frac{W}{U}\right)^2}{(1-\lambda)\left(\frac{W}{U}\right)^2} , \tag{42}$$

the result is obtained,

$$C_{p_m} = \frac{2}{M^2} \left[1 - \left(\frac{1-\lambda}{1+\lambda}\right) \frac{(1+\lambda)\left(\frac{W}{U}\right)^2}{(1-\lambda)\left(\frac{W}{U}\right)^2} \right] . \tag{43}$$

This reduces to the final result,

$$C_{p_m} = \frac{C_{p_i}}{\sqrt{1 - M^2} + \frac{M^2}{\sqrt{1 - M^2} + 1} \left(\frac{C_{p_i}}{2}\right)} . \tag{44}$$

It is important to remember that this equation is based on two assumptions. The first of these was the approximation of the isentrope by a straight line tangent at the point, p_∞, ρ_∞. The second assumption consisted of neglecting the change in boundary conditions in the compressible physical plane as compared with the incompressible physical plane. There is some reason to believe that the errors caused by these assumptions tend to balance each other out, since attempts to improve upon only one of them have actually resulted in larger errors (6, p.186).

C. Summary.

Two expressions have now been derived that show the relationship between the pressure coefficient in a compressible flow and the pressure coefficient in an incompressible flow. These are not the only solutions to the problem. At the present time there are other methods. An examination of these, however, reveals that the two foregoing approximate methods are the only ones of any engineering importance in regard to determining the pressure distribution over the airfoil. Most of the more complicated solutions reduce to the Prandtl-Glauert form for the first approximation, and become so complicated and tedious for the higher approximations that they, as yet, have not been completed for any airfoil shape. For this reason the Prandtl-Glauert and Karman-Tsien methods were chosen for this investigation.

It is interesting to note that the Karman-Tsien relationship (equation 44) will reduce to the Prandtl-Glauert formula (equation 26) for small values of C_{p_i} or M. The difference in the two relations will occur when C_{p_i} has a negative value and the denominator of equation (44) will be smaller than the denominator of equation (26). Thus, the Karman-Tsien formula will predict higher negative pressure coefficients than will the Prandtl-Glauert formula. This will become more apparent in the following sections.

V. PROCEDURE FOR CALCULATIONS

A. General.

Most methods of solution of subsonic, compressible aerodynamics problems are based on a correction of the incompressible solution, which can be determined. This investigation was carried out with the idea of calculating an analytic solution to the problem without the use of any experimental data. It is obvious, however, that the final compressible results can agree no better with experimental data than the theoretical incompressible calculations agree with incompressible experimental data. Therefore, in this section, the method in which the calculations were carried out will be covered, along with a brief coverage of the incompressible solution and the method that was used to get comparable results. It should be noted at this point that all calculations were carried out with a

slide rule. Because of this, the accuracy is somewhat limited, but is sufficient to show the desired results. Three significant figures are carried throughout the calculations.

B. The Incompressible Solution.

The method used in this investigation for determining the incompressible pressure distribution about the NACA 4412 airfoil is one of the most recent and most accurate methods available. The original paper on this method contains extensive data for the NACA 4412 airfoil, which reduces the calculations to a considerable degree. Basically, this method is developed on the following theory (1, p.1). The velocity distribution over an airfoil may be considered to consist of two effects. These effects are due to the camber and the base profile of the airfoil. The base profile of the airfoil is defined as the profile of the airfoil if the camber were removed and the resulting symmetrical airfoil set at zero angle of attack.

First, let us consider the effect of camber. The velocity distribution of the camber is dependent upon the shape of the mean line and its angle of attack. The mean camber is considered to be an infinitesimally thin line, and the velocity distribution is calculated on this camber-line by replacing it with a vortex system. The result of this is an expression of the difference in pressure coefficients, P, between the upper and lower surfaces in a Fourier series. The series has two types of terms. The first type is

independent of the shape of airfoil and dependent upon the angle of attack. The second type is solely dependent of the shape of the camber line. Each of these is then corrected for the effect of thickness and the result is P_b, the difference in upper and lower pressure coefficients due to the basic lift. Next, the C_l value for P_b (denoted by C_{l_b}) is determined and the additional P due to angle of attack corresponding to a given C_l is determined by correcting the P_a (already corrected for thickness) by the expression,

$$P_{a_{C_l}} = \frac{P_a}{C_{l_a}} (C_l - C_{l_b}), \tag{45}$$

where C_{l_a} is the coefficient of lift due to P_a. $\frac{P_a}{C_{l_a}}$ is calculated by first determining $\frac{{}_oP_a}{{}_oC_{l_a}}$ for infinitesmal thickness (denoted by o in front of P and C_{l_a}) and ${}_oC_{l_a} = 1$. Then this value of P_a is corrected to the finite thickness and the C_{l_a} is determined from this corrected P_a. Finally, the P due to the sum of the basic camber line and the additional lift is the total camber effect, or,

$$P_{C_l} = P_b + \frac{P_a}{C_{l_a}} (C_l - C_{l_b}). \tag{46}$$

The second effect on the airfoil is that of the base profile. The velocity distribution contributed by this is found by adding the known velocity distribution over some reference base profile having the same leading edge radius to the change in velocity distribution due to a change in shape from the reference to the

given base profile. This velocity distribution is non-dimensionally expressed as $\frac{w_f}{U}$.

Knowing the chordwise P distribution due to the camber line, and the chordwise velocity distribution due to the base profile, the upper and lower surface velocity distributions may be found by the superposition method (1, p.10) which gives,

$$\frac{w_u}{U} = \frac{w_f}{U} + \frac{\frac{P}{4}}{\frac{w_f}{U}}$$

$$\frac{w_\ell}{U} = \frac{w_f}{U} - \frac{\frac{P}{4}}{\frac{w_f}{U}} . \qquad (47)$$

Formulas (45), (46), and (47) are the ones that were used to carry out the incompressible calculations. Data for the NACA 4412 airfoil in the form of P_b, $\frac{P_a}{C_{\ell_a}}$ and $\frac{w_f}{U}$ are given (1, p.23) and the above calculations are easily carried out. The incompressible pressure coefficient may be found from the velocity distribution, for it may be shown using Bernoulli's equation for incompressible flow that,

$$C_{p_i} = 1 - \left(\frac{w}{U}\right)^2 . \qquad (48)$$

It is seen from equation (46) that the pressure and consequently the velocity distribution around the airfoil is determined by the C_ℓ of the section. Thus, in order to compare the results of the calculations with existing data on the subject,

the same C_l values must be used as in the experimental work. However, in the experimental work, the airfoil was placed at a given angle of attack, α, in a compressible flow. To be exact, the experimental data for the NACA 4412 airfoil (8, p.78) is presented for three angles of attack and for various Mach numbers at each angle of attack. It was decided at this point to carry out the theoretical calculations for the two highest angles of attack of the experimental data; namely, $\alpha = -0.25°$ and $\alpha = 1.88°$ for four Mach numbers each. These four Mach numbers were not the same for both angles of attack due to the irregularity of the experimental data. Fortunately, at least one of the Mach numbers for each angle of attack in the experimental data was so low that it could be considered almost incompressible. In order to compare these low Mach number data with the incompressible flow, equation (26) was used to correct the experimental data to $M = 0$. Since for both of the above angles of attack, experimental data was available at $M < 0.2$, the corresponding correction from (26) would be,

$$C_{p_i} \leq 0.96\, C_{p_m} . \tag{49}$$

Thus, it is seen that the difference between C_{p_i} and C_{p_m} is very small, for this Mach number. Since past experience indicates that equation (26) is good at very low Mach numbers, it was used to determine the incompressible experimental pressure distribution. The calculations for this appear in Table I ($\alpha = -0.25°$) and

Table VII ($\alpha = 1.88°$) in the Appendix and the results are plotted in Figure 6 ($\alpha = -0.25°$) and Figure 7 ($\alpha = 1.88°$).

At first it was thought that the C_ℓ of the experimental incompressible pressure distribution could be determined by the fundamental aerodynamic relationship,

$$C_\ell = m(\alpha - \alpha_{C_\ell=0}), \tag{50}$$

where m is the slope of the lift curve and $\alpha_{C_\ell=0}$ is the zero lift angle. Calculations were made using equation (50) and the resulting C_ℓ values were used to calculate the theoretical pressure distribution discussed in the first part of this section. However, when the calculated incompressible pressure distribution was plotted for comparison with the corrected experimental distribution, the results were highly unsatisfactory. Comparison was poor and the C_ℓ values did not agree even though they were supposedly the same as determined by equation (50). This method was then abandoned. It was decided to use the C_ℓ from the corrected experimental incompressible pressure distribution which was obtained by the mechanical integration of the approximate equation (7, p.140),

$$C_\ell = \frac{1}{C}\int_0^C \left(\frac{\Delta p}{q}\right)dx. \tag{51}$$

The C_ℓ determined from Figure 6 ($\alpha = -0.25°$, corrected experimental) was 0.461, and the C_ℓ determined from Figure 7 ($\alpha = 1.88°$, corrected experimental) was 0.687. These C_ℓ values were used for calculating the theoretical incompressible pressure

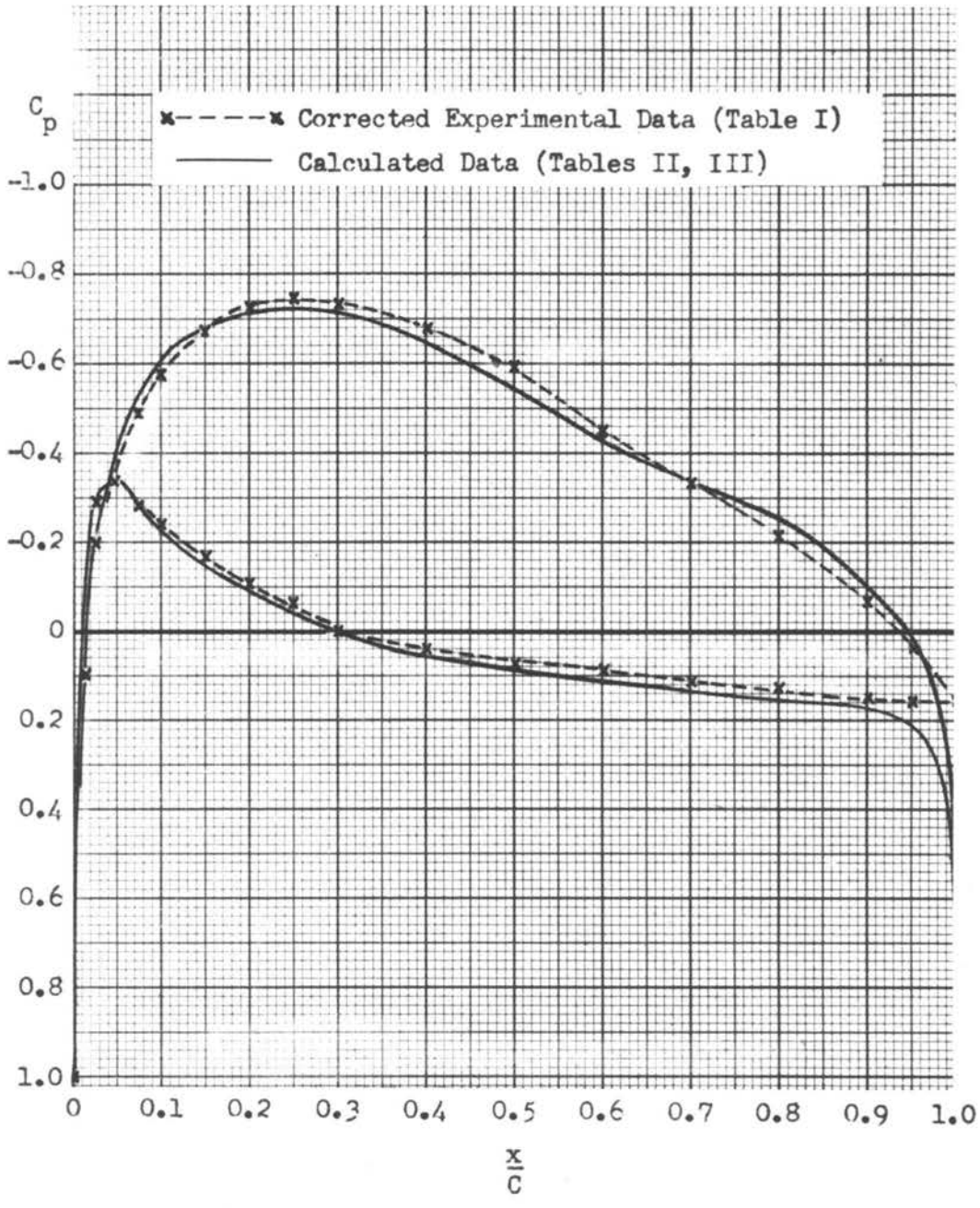

Figure 6.

Incompressible Pressure Distribution for $\alpha = -0.25°$.

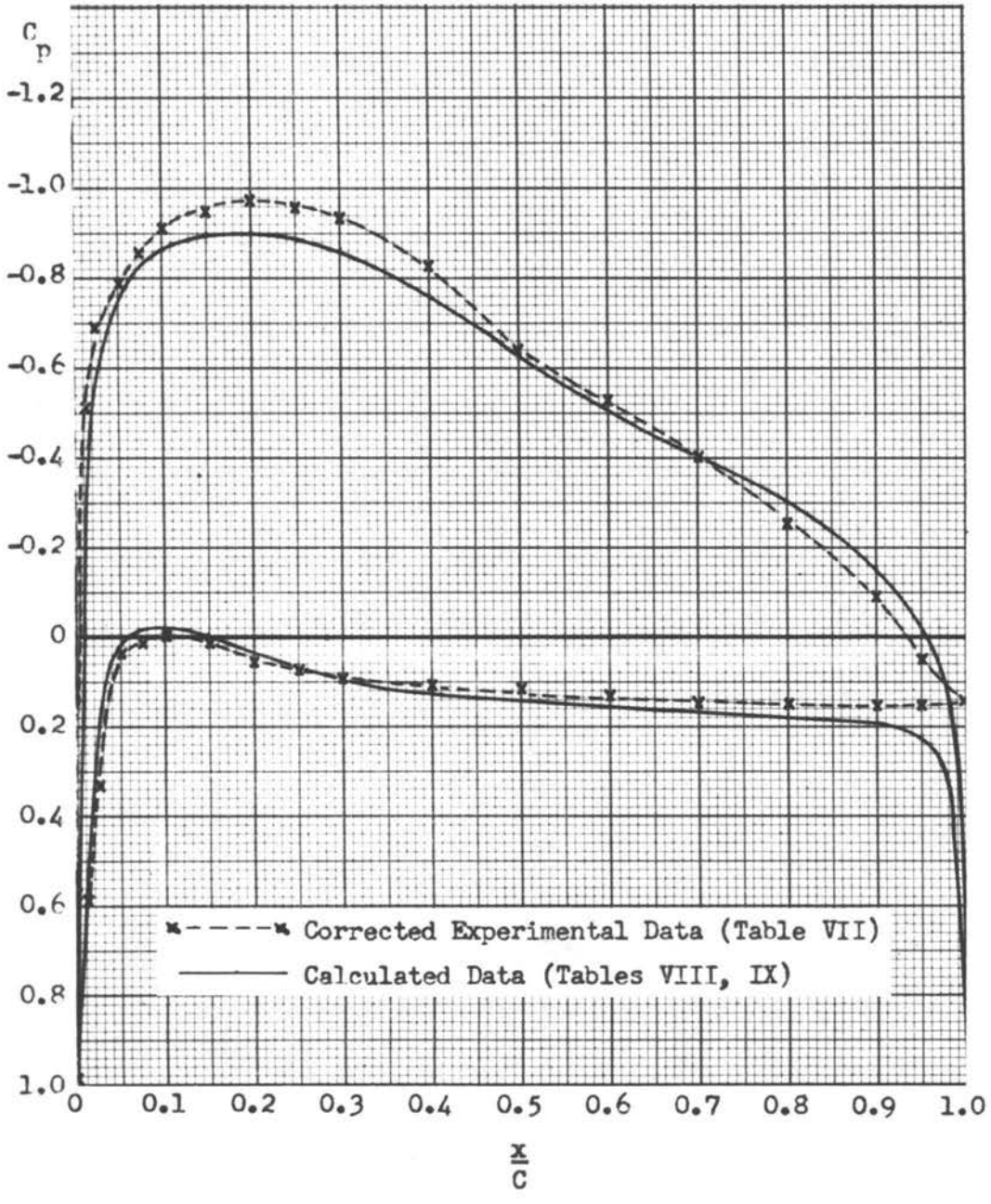

Figure 7.

Incompressible Pressure Distribution for $\alpha = 1.88°$.

as before, and the results were again plotted with the experimental. This time good agreement was obtained. The complete theoretical incompressible calculations for these are presented in Tables II and III ($\alpha = -0.25°$), and Tables VIII and IX ($\alpha = 1.88°$). These are the theoretical results which are compared with the experimental data in Figures 6 and 7. The curves show good agreement in both cases except near the maximum C_p value in Figure 7. These comparisons are an important part of the procedure, for it should be remembered that no better compressible agreement can be shown than is exhibited between the incompressible distributions using the methods of this report.

C. The Compressible Solution.

Thus far the incompressible solution for the airfoil has been determined at two angles of attack. The next step was to calculate the compressible pressure distribution using equations (26) and (44). The Mach number chosen for these calculations coincided with the Mach numbers in the experimental data. Four Mach numbers were used for each angle of attack. For $\alpha = -0.25°$, the compressible calculations were carried out at Mach numbers of 0.299, 0.427, 0.517, and 0.590. For $\alpha = 1.88°$, calculations were carried out at Mach numbers of 0.512, 0.596, 0.640, and 0.735. These calculations were set up in tabular form and appear in the Appendix. Tables IV and X contain the calculations for the Prandtl-Glauert method at $\alpha = -0.25°$ and $1.88°$ respectively. In

the same manner, Tables V and XI contain the calculations for the Karman-Tsien method. For convenient reference, Tables VI and XII present the experimental data for both angles of attack. The results of the compressible calculations were plotted together with the experimental data for comparison.

D. Summary.

When speaking of the flow about an airfoil, one usually thinks of velocities. Depending upon what viewpoint is desired, the non-dimensional velocity, w/U, over the surface may be found if a physical picture of the flow is wanted. On the other hand, if one is more interested in forces, the pressure coefficients may be determined as in this investigation. The pressure coefficient is used in determining the C_ℓ values, in finding the center of pressure of a section, and in determining forces on an airfoil. In order to get an overall picture of the effects of compressibility, therefore, the C_ℓ values were determined for all pressure distributions (including experimental) using equation (51). These were plotted against Mach number. Also, to get an idea of how the maximum forces on the airfoil section compared as predicted by the two methods, the C_p value for the upper surface was plotted at 30 per cent chord, which is very nearly the maximum point. These curves, as well as the pressure distributions, will be discussed in the following section.

VI. RESULTS

A. General.

In the pressure distributions (C_p versus $\frac{x}{C}$), the negative values of C_p are on the upper portion of the C_p axis and the positive values are on the lower. This is so the upper surface pressure distribution will appear on top. Thus, the curves of high negative value are for the upper surfaces, while the small negative and positive values are the lower surfaces. The difference between the upper and lower surfaces was not designated by a difference in curves because it was thought that this would only be confusing, with three different pressure distribution curves with each in two different parts. It is believed that there will be no difficulty in distinguishing between the upper and lower surface for each curve.

B. The Pressure Distributions.

The calculated distributions for $\alpha = -0.25^\circ$ appear in the order of increasing Mach number in Figures 8, 9, 10, and 11. Figures 8 and 9 show very good agreement between the experimental and the two methods of calculation. As the Mach number increases, however, there is seen to be a greater difference between the experimental and calculated values of C_p. This change takes place not only in the magnitude of the C_p values, but also in the occurence of the maximum C_p. The maximum value of the experimental

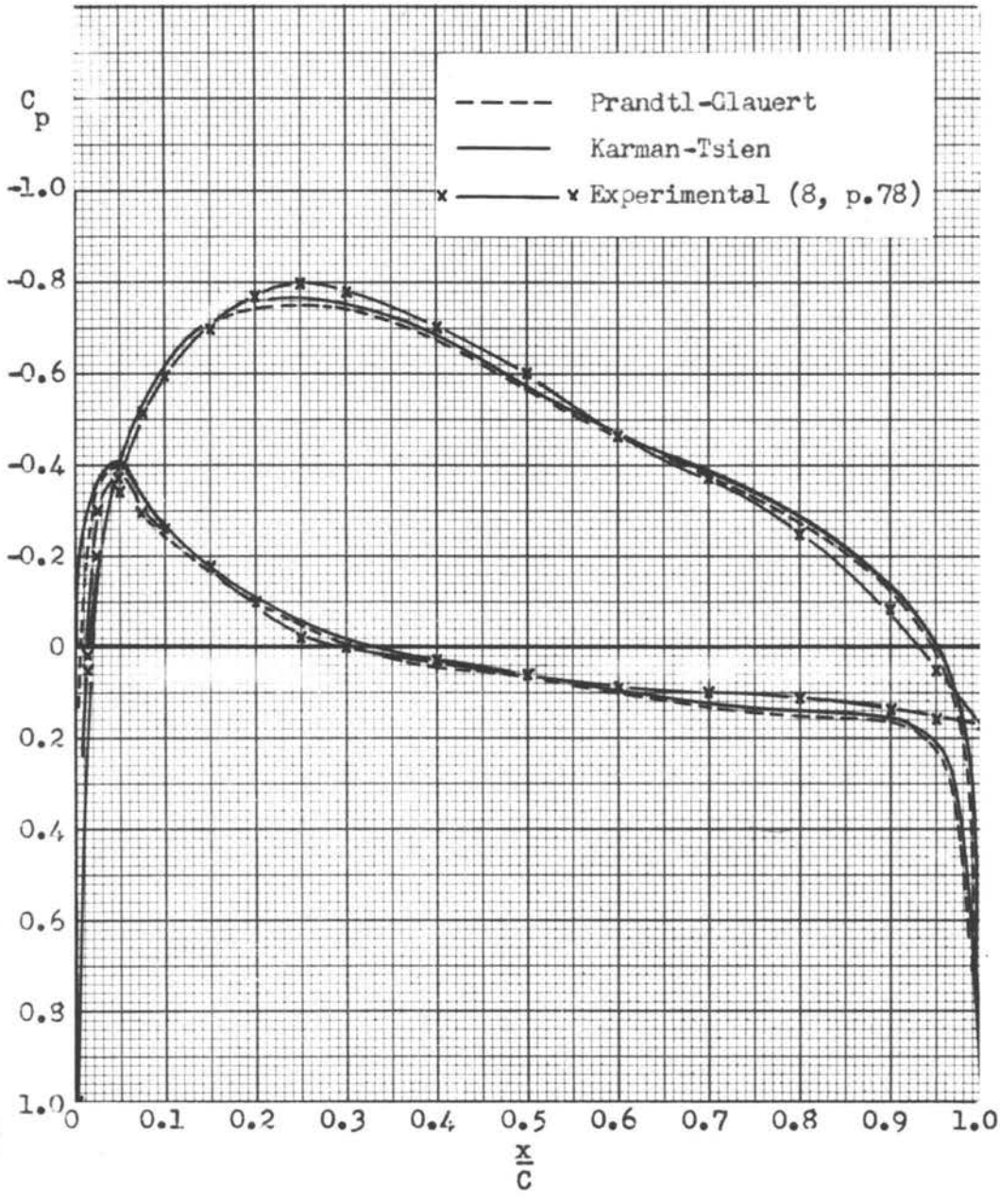

Figure 8.

Comparison of Pressure Distributions at $\alpha = -0.25°$, M = 0.299.

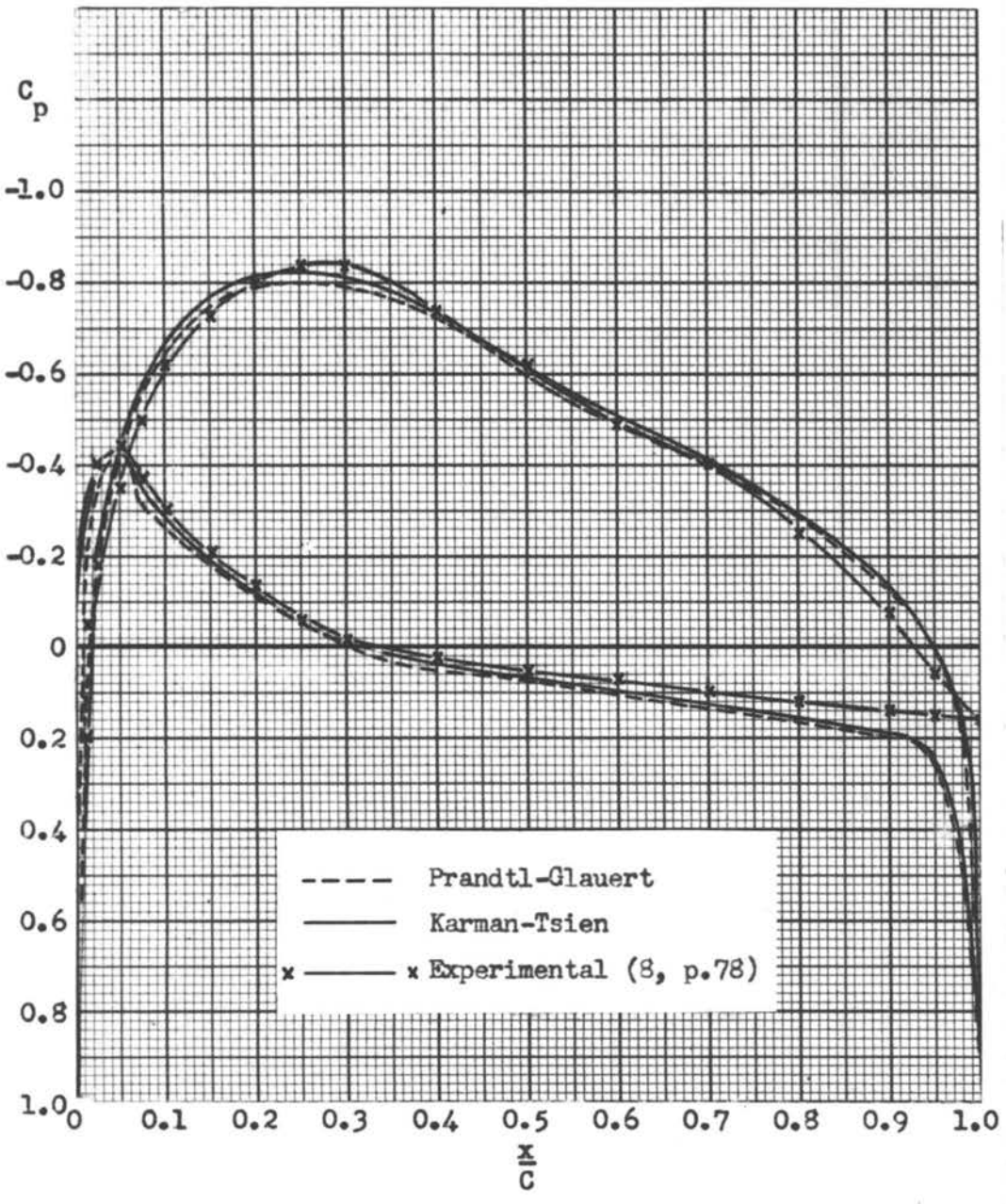

Figure 9.

Comparison of Pressure Distributions at $\alpha = -0.25°$, M = 0.427.

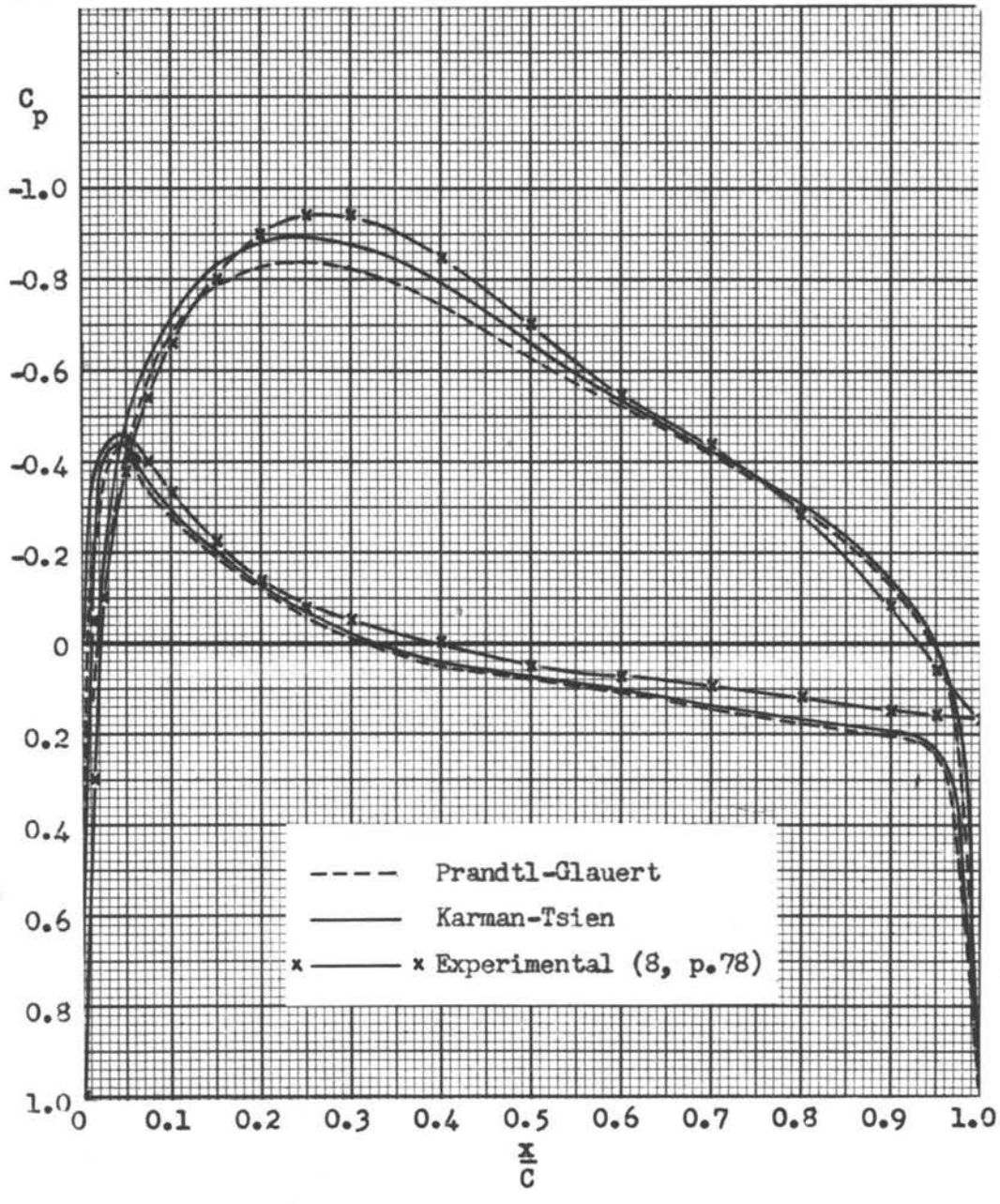

Figure 10.

Comparison of Pressure Distributions at
$\alpha = -0.25°$, $M = 0.517$.

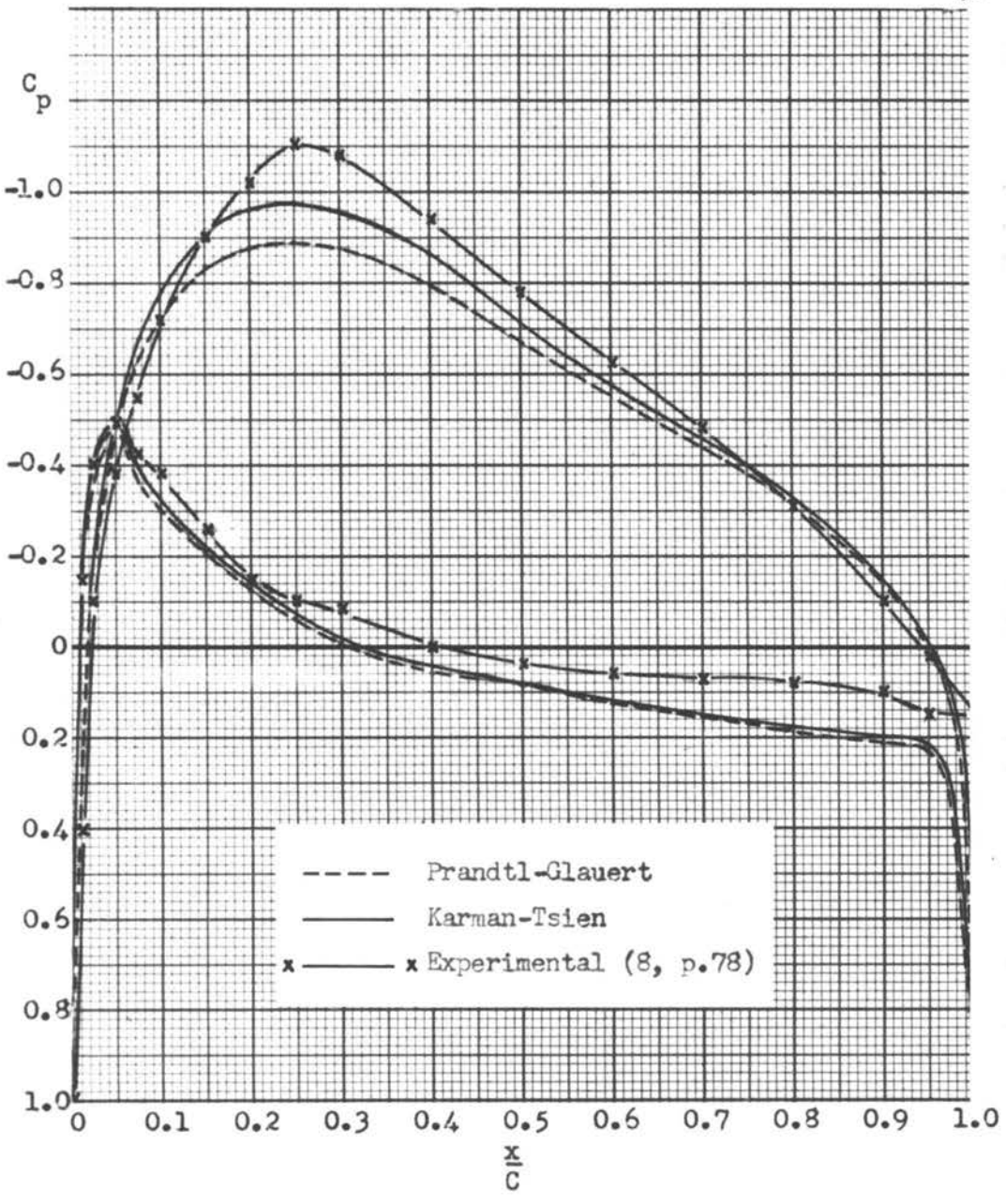

Figure 11.

Comparison of Pressure Distributions at
$\alpha = -0.25°$, $M = 0.590$.

C_p shows a tendency to shift toward the center of the chord. This fact will be even more pronounced in the case of the higher angle of attack. The major disagreement in magnitude occurs at about the 30 per cent chord point on the upper surface and near the trailing edge on the lower surface. While the experimental values remain almost constant at and near the trailing edge on the lower surface, the calculated values become greater and greater with the higher Mach numbers. This causes a considerable disagreement at the higher values of Mach number.

For incompressible flow, it may be shown from Bernoulli's equation that at stagnation points, $C_p = 1$. Stagnation points occur at the leading edge and the trailing edge. However, the theory from which the incompressible flow was calculated results in an indeterminate expression at these points, so no C_{p_m} are calculated at these points from the Prandtl-Glauert or Karman-Tsien methods. However, since a C_p of one is predicted for the incompressible, there cannot be too much error in assuming that the theoretical C_p at these points would be near to one. Actually, the curves were drawn as being asymptotic to the C_p axes at those points. The question is purely academic, however, for the area enclosed is so small as to be considered negligible. The difference between the calculated and experimental C_Q's due to this fact is not enough to be considered important. The important thing to note is the fact that the Karman-Tsien method gives a closer approximation to the experimental value than does the

Prandtl-Glauert, although both tend to underestimate the effects at higher Mach numbers. As corrections to the incompressible distributions, neither method can predict changes in the shape of the distribution, but only serve to magnify the incompressible distributions.

The comparison of pressure distribtuions for $\alpha = 1.88°$ is shown in Figures 12, 13, 14, and 15. The higher angle of attack results in higher C_{p_i} values. The combination of this and the higher Mach numbers at this angle of attack causes the flow to go over the critical pressure coefficient. The critical pressure coefficient is defined as the pressure coefficient at which the local velocity is equal to the speed of sound. The C_{p_c} values are ruled in on Figures 13, 14, and 15. These values are determined (8, p.76) by the relation,

$$C_{p_c} = \frac{0.528\, p_o - p_\infty}{q_\infty} . \qquad (52)$$

At this point, it must be noted that the theory fails after the critical has been reached. If a sudden pressure jump, such as a shock wave, occurs, as in Figures 14 and 15 (indicated on the experimental curve by portion of curve between small arrows), the flow will no longer be reversible adiabatic and one of our basic assumptions will not hold. However, it is interesting to see how the theory agrees. Much of the same effect is found at the higher Mach numbers and angles of attack as was experienced at the lower

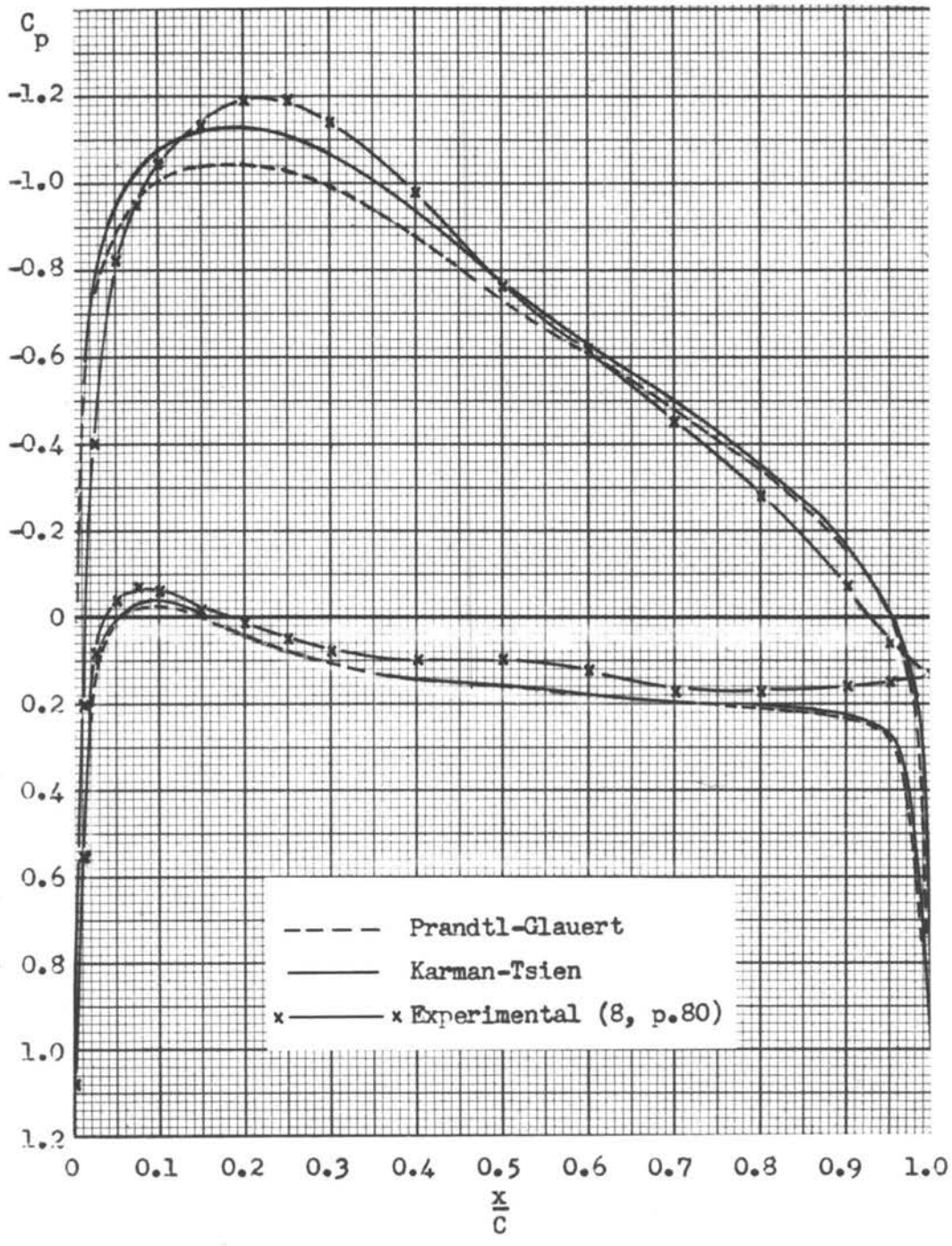

Figure 12.

Comparison of Pressure Distributions at $\alpha = 1.88°$, $M = 0.512$.

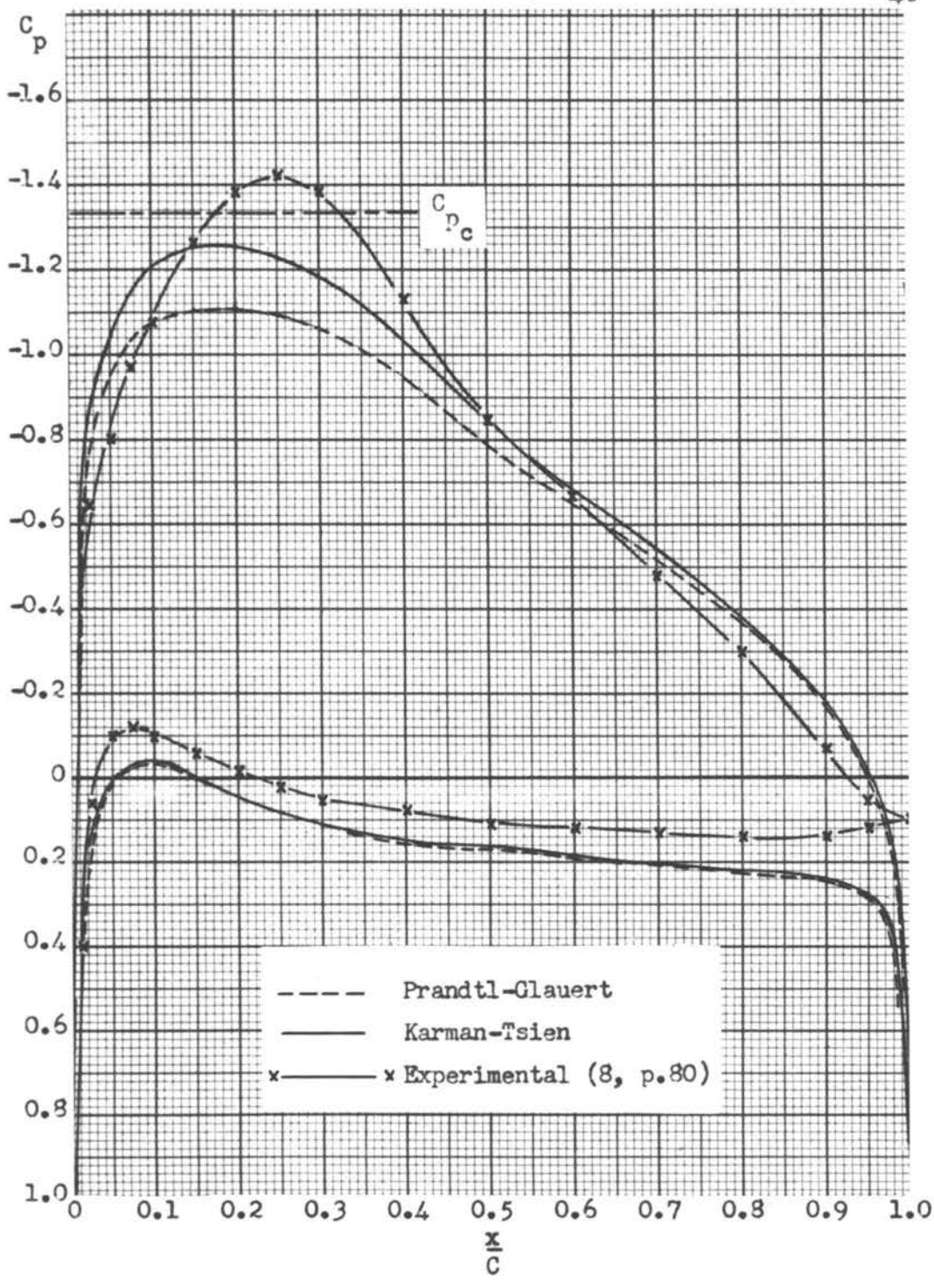

Figure 13.

Comparison of Pressure Distributions at $\alpha = 1.88°$, $M = 0.596$.

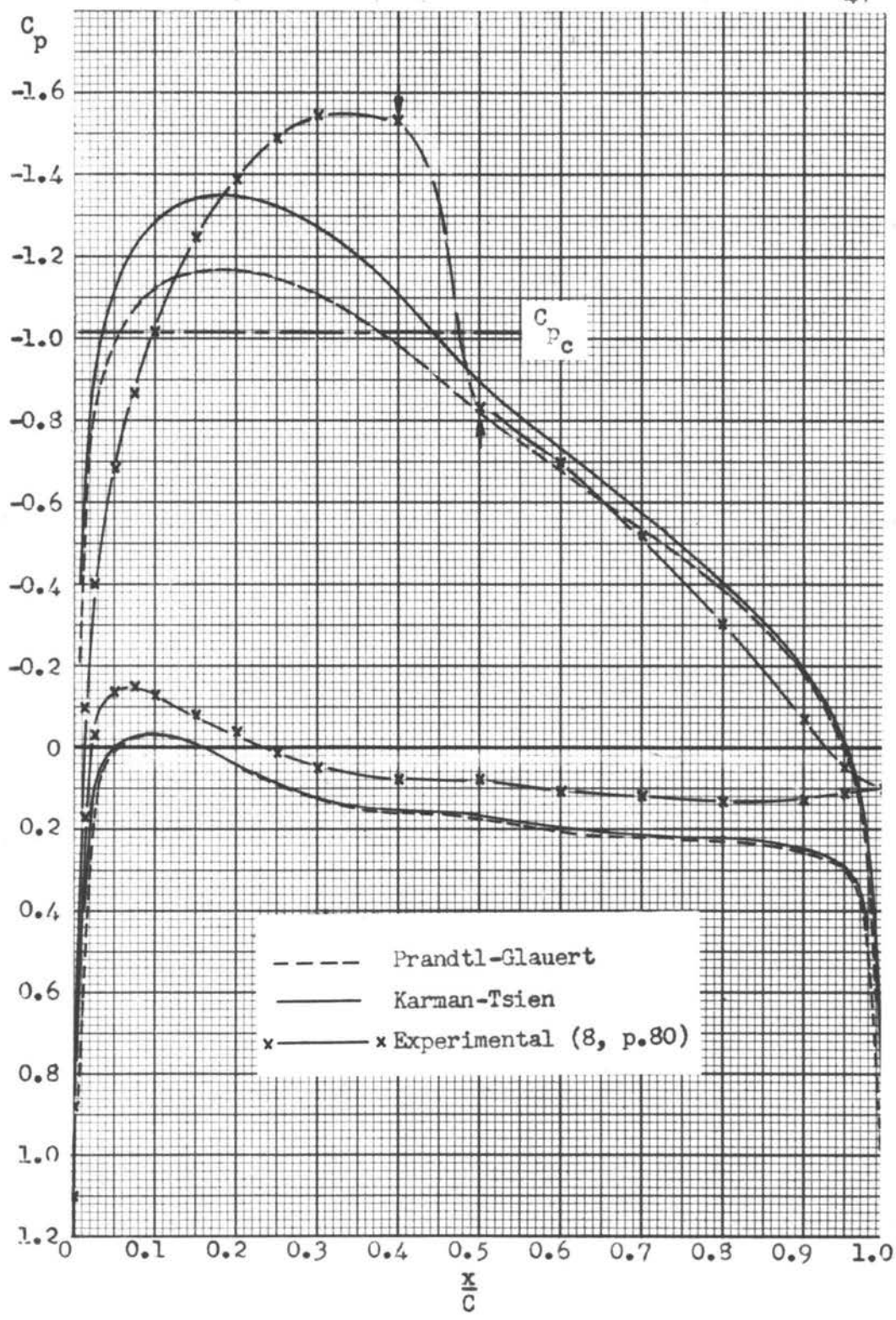

Figure 14.

Comparison of Pressure Distributions at
α = 1.88°, M = 0.640.

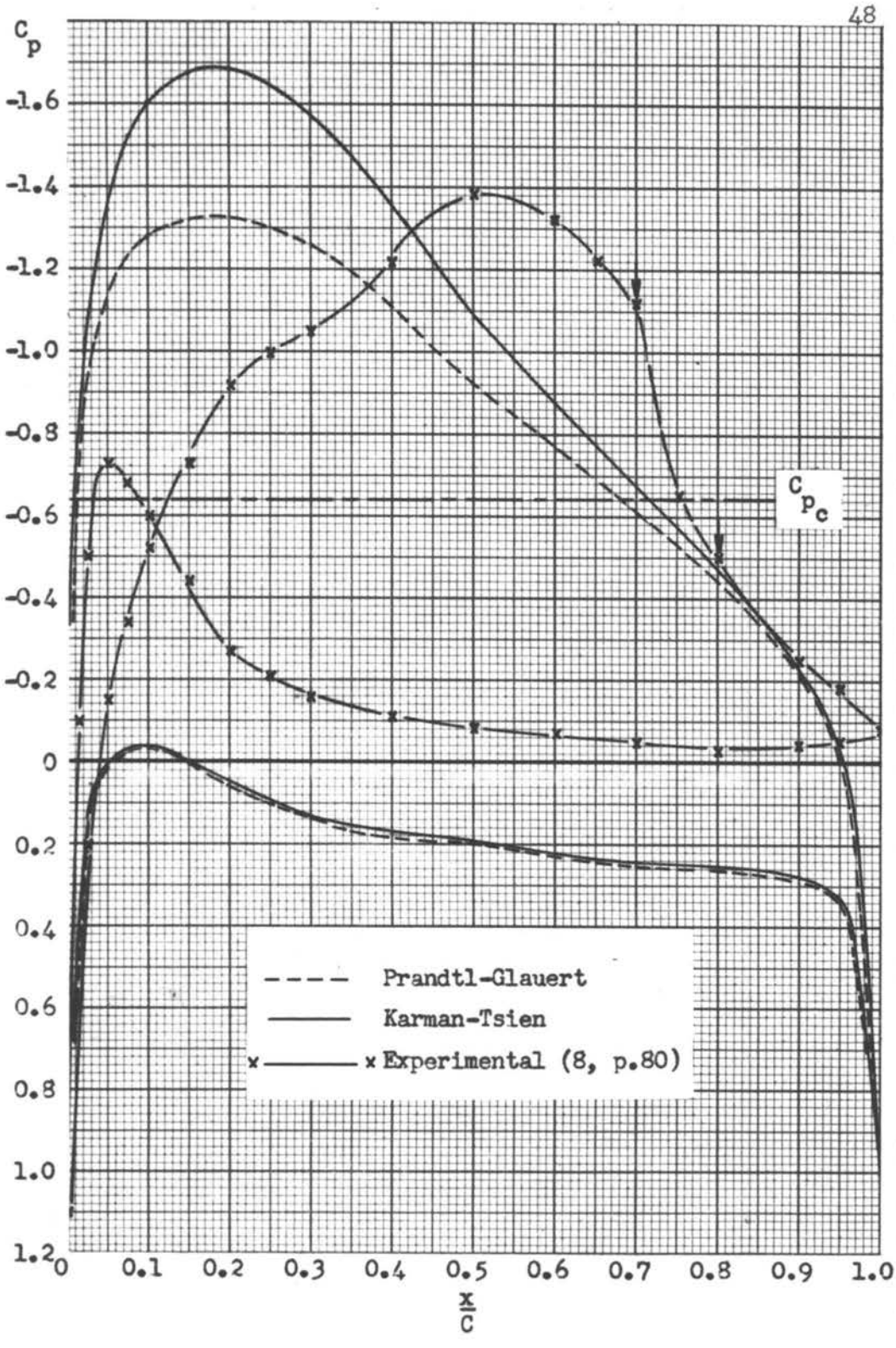

Figure 15.

Comparison of Pressure Distributions at
$\alpha = 1.88°$, $M = 0.735$.

angle of attack.

The effects of the compressibility are much more pronounced. Here, the shift of the maximum megative pressure coefficient is definite. In Figure 14 ($M = 0.640$), the maximum experimental C_p occurs at about 20 per cent chord, while the theoretical methods predict the maximum between 10 per cent and 15 per cent. In Figure 15 ($M = 0.735$), the experimental maximum occurs at 50 per cent, while the theoretical methods still predict 10 per cent to 15 per cent. As it will soon be shown, this last Mach number is past the "compressibility stall", so-named because of the similar loss of lift that occurs at excessive angles of attack.

The importance of angle of attack can be seen from the pressure distributions. Even at $\alpha = 1.88°$, critical conditions occur over the airfoil at $M = 0.596$. The reason for this is partly due to the airfoil. More efficient, high-critical-C_p airfoils are now being designed and used in actual practice. One other discrepancy that causes undesirable results is the fact that the incompressible experimental and incompressible theoretical distributions differ to a great extent at the maximum negative C_p value (see Figure 7). This is responsible to a large degree for the discrepancies in the compressible distributions.

C. The Effects of Mach Number on Maximum C_p and on C.

In order to get a better picture of what happens to the C_p

values as Mach number is increased, Figure 16 was plotted. This figure shows the variation of the C_p at 30 per cent chord on the upper surface with increasing Mach numbers. The 30 per cent chord point represents close to the maximum except in the case of the higher Mach numbers. The results of the calculations for both angles of attack are plotted. For $\alpha = -0.25°$, the Karman-Tsien relation gives the best approximation. At $M = 0.590$, the Karman-Tsien method is 10 per cent in error and the Prandtl-Glauert method is 20 per cent in error. For the higher angle of attack, $\alpha = 1.88°$, two things are immediately seen. The first of these is the disagreement in the incompressible C_p values. If the experimental C_{p_i} and the calculated C_{p_i} had been in better agreement, it appears that the Karman-Tsien method might have given a very good approximation. The second important point to notice is the sudden drop in experimental C_p after $M = 0.640$ has been reached. This sudden drop of C_p comes from the break in flow described in the foregoing section, and is responsible for the "compressibility stall."

Figure 17 shows the relationship between C_ℓ and Mach number at the two angles of attack. These C_ℓ values were found by mechanical integration of the approximate equation (51). The calculation appears as Table XIII in the Appendix. The results of it are not in agreement with the general opinions expressed in literature on the subject, for in both cases the two approximate methods give higher C_ℓ values than the experimental values.

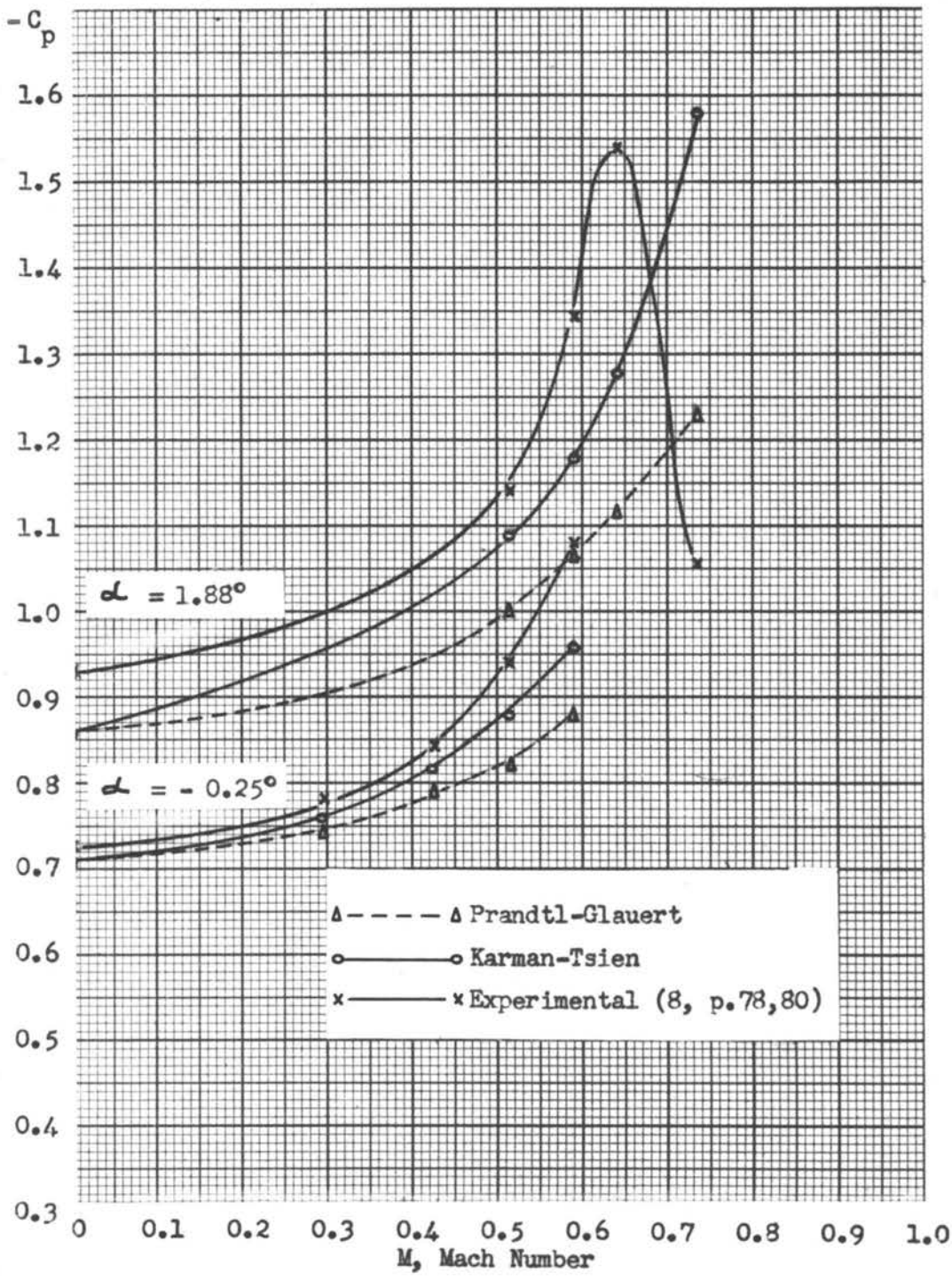

Figure 16.

Comparison of Pressure Coefficient at 30% Chord.

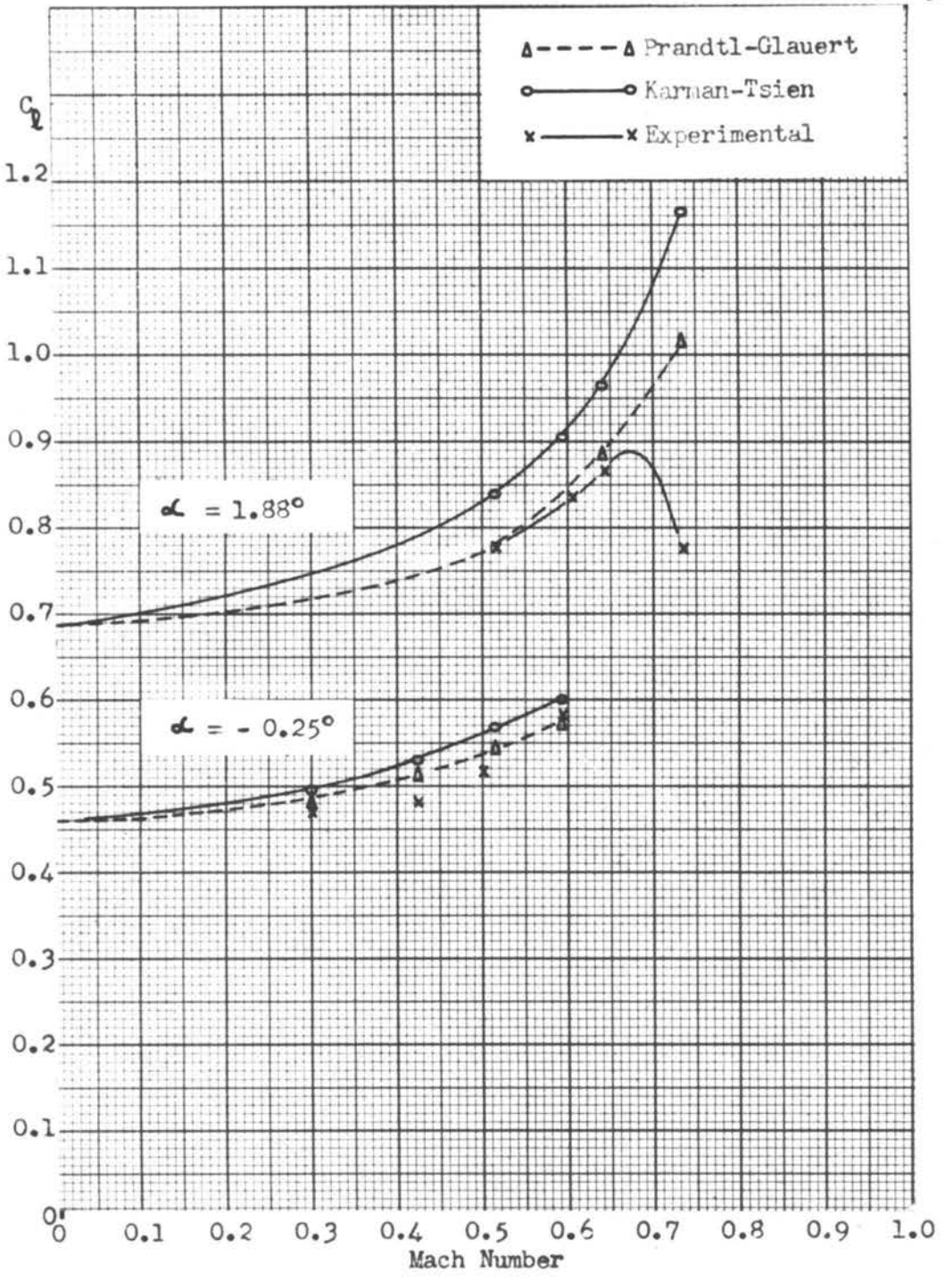

Figure 17.

Comparison of Lift Coefficients.

However, the author has not found any direct calculations of this sort in the literature to compare with Figure 17. For = 1.88°, the "compressibility stall" is clearly shown by the experimental data. The reasons for the higher theoretical values were the disagreement in the pressure distribution on the lower surface of the airfoil. This discrepancy at both angles of attack more than counteracted the maximum C_p values, which fall exactly as they are predicted by existing literaure, to give the higher C values for the theoretical calculations.

D. Summary.

In general, the results are not extensive enough to show any special trends. However, the author does not believe that either of these methods is satisfactory for the speed range $U_c/2$ to U_c. The results show that the Prandtl-Glauert method is good only at Mach numbers less than 0.500. The Karman-Tsien method will give better agreement, however, and might be used as a general indication of compressibility effects up to the critical condition. Whenever the above methods are used, the angle of attack must be small for good results. This limitation, plus the inability to predict shifts in the center of pressure of the distribution, leave much to be desired in using the above methods.

The results do show some advantages, however. The most significant of these is the ease of application. Both may be applied with a minimum of tedious calculations and do not require extreme lengths of time. This would be of importance in

engineering work. Even though the methods do not show excellent agreement with experiment, they would serve well as a first approximation in a more complicated procedure.

VII. CONCLUSIONS

Although the investigation was carried out with the idea of calculating compressible flow completely without the aid of experiment, it was shown in the results that one of the major difficulties was in acquiring an accurate incompressible solution. For this reason, it is recommended that the methods in this report be applied to experimental incompressible data when available. It is believed that in this way much better results would be obtained. This, of course, would partially defeat the purpose of saving the high experimental costs that occur in this work.

Actually, the investigation has not produced the results originally hoped for. Neither of the solutions presented gives a satisfactory final answer to the problem at hand. However, they represent the only quick and practicable methods of approach to the problem at the present time.

The future outlook for the problem is far from hopeless, however. After a major part of the work in this investigation had been completed, a paper was found on the subject which utilized Southwell's relaxation method (3, p.1). Time did not permit inclusion of this in the work, but a numerical solution such as

this, or a numerical integration method as applied to the equations of flow might have good possibilities. Future work on this two-dimensional, subsonic, flow problem would certainly be of great importance to the field of aerodynamics, for although many have contributed to the theory, there still remains to be found an accurate solution for an arbitrary profile. Success in this field of research would mean great advances in modern, high-speed airplane design.

VIII. BIBLIOGRAPHY

1. Allen, H. General theory of airfoil sections having arbitrary shape or pressure distribution. NACA TR 833, 1945. 23p.

2. Chaplygin, A. Gas jets. NACA TM 1063, 1944. 112p.

3. Emmons, H. W. The numerical solution of compressible fluid flow problems. NACA TN 932, May 1944. 50p.

4. Glauert, H. The effect of compressibility on the lift of an airfoil. R. & M. No. 1135, British A.R.C., 1927. 7p.

5. Jacobs, E., Ward, K. and Pinkerton, R. The characteristics of 78 related airfoil sections from tests in the variable density wind tunnel. NACA TR 460, 1933. 54p.

6. Liepmann, H. and Puckett, A. Introduction to aerodynamics of a compressible fluid. New York, John Wiley and Sons, Inc., 1947. 262p.

7. Pope, A. Wind tunnel testing. New York, John Wiley and Sons, 1947. 319p.

8. Stack, J., Lindsey, W. and Littel, R. The compressibility burble and the effects of compressibility on the pressure and forces acting on an airfoil. NACA TR 646, 1939. 23p.

9. Stack, J. Compressibility flows in aerodynamics. Journal of the aeronautical sciences, vol.12, no. 2, April 1945. 16p.

10. Sibert, H. High speed aerodynamics. New York, Prentice Hall, Inc., 1948. 299p.

11. Tsien, H. and Lees, L. The Glauert-Prandtl approximation for subsonic flows of a compressible fluid. Journal of the aeronautical sciences, vol.12, 1945. 14p.

12. von Karman, Th. Compressibility effects in aerodynamics. Journal of aeronautical sciences, vol.8, no. 9, 1941. 20p.

TABLE I

CALCULATION OF EXPERIMENTAL PRESSURE DISTRIBUTION AT $\alpha = -0.25°$

(Correction of Experimental C_{p_m} at M = 0.141 to C_{p_i} at M = 0).

(By the Relation, $C_{p_i} = \beta C_{p_m}$; $\beta = 0.992$).

$\frac{x}{C}$	# M = 0.141		M = 0	
	$C_{p_{u_m}}$	$C_{p_{l_m}}$	$C_{p_{i_u}}$	$C_{p_{i_l}}$
0.0000	1.000	1.000	1.000	1.000
0.0125	0.100	0.020	0.099	0.0198
0.0250	-0.200	-0.300	-0.190	-0.296
0.0500	-0.350	-0.340	-0.348	-0.337
0.0750	-0.500	-0.280	-0.496	-0.278
0.1000	-0.580	-0.240	-0.575	-0.238
0.1500	-0.680	-0.170	-0.674	-0.168
0.2000	-0.730	-0.110	-0.724	-0.109
0.2500	-0.750	-0.070	-0.744	-0.069
0.3000	-0.740	0.000	-0.734	0.000
0.4000	-0.680	0.040	-0.675	0.040
0.5000	-0.600	0.070	-0.595	0.069
0.6000	-0.450	0.085	-0.446	0.084
0.7000	-0.340	0.115	-0.337	0.114
0.8000	-0.220	0.125	-0.218	0.124
0.9000	-0.075	0.150	-0.074	0.149
0.9500	0.040	0.160	0.040	0.159
1.0000	0.150	0.150	0.149	0.149

Data from (8, p.78)

TABLE II

VELOCITY DISTRIBUTION CALCULATION FOR NACA 4412 AIRFOIL AT $C_\ell = 0.461$ ($\alpha = -0.25°$).
(Incompressible Flow)

$$\eta = (C_\ell - C_{\ell_b}) = (0.461 - 0.587) = -0.126$$

$\frac{x}{C}$	# P_b (C_ℓ=0.587)	# $\frac{P_a}{C_{\ell_a}}$	$\frac{P_a}{C_{\ell_a}}(\eta)$	P (C_ℓ=0.461)	$\frac{w_f}{U}$	$P/4/w_f/U$	$\frac{w_u}{U}$	$\frac{w_\ell}{U}$
0.0000	0.000	0.000	0.000	0.000	0.000	---	---	---
0.0125	0.271	5.408	-0.683	-0.412	0.987	-0.104	0.883	1.091
0.0250	0.355	4.235	-0.534	-0.179	1.099	-0.041	1.058	1.140
0.0500	0.472	3.126	-0.394	-0.078	1.163	-0.017	1.146	1.180
0.0750	0.554	2.560	-0.323	0.231	1.181	0.049	1.230	1.132
0.1000	0.620	2.199	-0.277	0.343	1.188	0.072	1.260	1.116
0.1500	0.724	1.742	-0.219	0.505	1.187	0.106	1.293	1.081
0.2000	0.792	1.454	-0.183	0.609	1.179	0.129	1.308	1.050
0.2500	0.828	1.248	-0.157	0.671	1.168	0.144	1.312	1.024
0.3000	0.841	1.090	-0.137	0.704	1.156	0.152	1.308	1.004
0.4000	0.802	0.854	-0.108	0.694	1.129	0.154	1.283	0.975
0.5000	0.694	0.681	-0.086	0.608	1.103	0.138	1.241	0.965
0.6000	0.622	0.542	-0.068	0.554	1.076	0.129	1.205	0.947
0.7000	0.543	0.424	-0.054	0.489	1.050	0.116	1.166	0.934
0.8000	0.451	0.315	-0.040	0.411	1.022	0.101	1.123	0.921
0.9000	0.320	0.202	-0.025	0.295	0.982	0.075	1.057	0.907
0.9500	0.227	0.134	-0.017	0.210	0.942	0.056	0.998	0.886
1.0000	0.000	0.000	0.000	0.000	0.000	---	---	---

#Data from (1, p.23)

TABLE III

CALCULATION OF INCOMPRESSIBLE PRESSURE DISTRIBUTION FOR NACA 4412 AIRFOIL AT $C_l = 0.461$ ($\alpha = -0.25°$).

$\frac{x}{c}$	$(\frac{w_u}{U})^2$	$(\frac{w_l}{U})^2$	$C_{p_{u_i}} = 1-(\frac{w_u}{U})^2$	$C_{p_{l_i}} = 1-(\frac{w_l}{U})^2$
0.0000	---	---	---	---
0.0125	0.780	1.191	0.220	-0.191
0.0250	1.120	1.300	-0.120	-0.300
0.0500	1.315	1.390	-0.315	-0.390
0.0750	1.515	1.280	-0.515	-0.280
0.1000	1.580	1.240	-0.580	-0.240
0.1500	1.675	1.167	-0.675	-0.167
0.2000	1.710	1.100	-0.710	-0.100
0.2500	1.720	1.048	-0.720	-0.048
0.3000	1.710	1.008	-0.710	-0.008
0.4000	1.645	0.951	-0.645	0.049
0.5000	1.540	0.931	-0.540	0.069
0.6000	1.450	0.899	-0.450	0.101
0.7000	1.357	0.873	-0.357	0.127
0.8000	1.260	0.848	-0.260	0.152
0.9000	1.117	0.823	-0.117	0.177
0.9500	0.995	0.785	0.005	0.215
1.0000	---	---	---	---

TABLE IV

CALCULATION OF COMPRESSIBLE PRESSURE DISTRIBUTION FOR NACA 4412 AIRFOIL AT $\alpha = -0.25°$ USING PRANDTL-GLAUERT METHOD.

$$C_{p_m} = \frac{C_{p_i}}{\beta}$$

$\frac{x}{C}$	Incompressible		M = 0.299		M = 0.427		M = 0.517		M = 0.590	
			β = 0.955		β = 0.905		β = 0.858		β = 0.809	
	$C_{p_{u_i}}$	$C_{p_{l_i}}$	$C_{p_{u_m}}$	$C_{p_{l_m}}$	$C_{p_{u_m}}$	$C_{p_{l_m}}$	$C_{p_{u_m}}$	$C_{p_{l_m}}$	$C_{p_{u_m}}$	$C_{p_{l_m}}$
0.0000	---	---	---	---	---	---	---	---	---	---
0.0125	0.220	-0.191	0.230	-0.200	0.243	-0.211	0.256	-0.222	0.272	-0.236
0.0250	-0.120	-0.300	-0.126	-0.314	-0.133	-0.332	-0.140	-0.350	-0.148	-0.371
0.0500	-0.315	-0.390	-0.330	-0.408	-0.348	-0.431	-0.367	-0.454	-0.389	-0.482
0.0750	-0.515	-0.280	-0.539	-0.293	-0.569	-0.309	-0.600	-0.326	-0.636	-0.348
0.1000	-0.580	-0.240	-0.608	-0.252	-0.640	-0.266	-0.675	-0.280	-0.716	-0.296
0.1500	-0.675	-0.167	-0.706	-0.175	-0.746	-0.185	-0.786	-0.195	-0.834	-0.206
0.2000	-0.710	-0.100	-0.744	-0.105	-0.785	-0.110	-0.826	-0.117	-0.877	-0.124
0.2500	-0.720	-0.048	-0.754	-0.050	-0.796	-0.053	-0.839	-0.056	-0.890	-0.059
0.3000	-0.710	-0.008	-0.744	-0.008	-0.785	-0.009	-0.826	-0.009	-0.877	-0.010
0.4000	-0.645	0.049	-0.675	0.051	-0.713	0.054	-0.751	0.057	-0.797	0.061
0.5000	-0.540	0.069	-0.566	0.072	-0.597	0.076	-0.629	0.080	-0.667	0.085
0.6000	-0.450	0.101	-0.471	0.106	-0.497	0.112	-0.524	0.118	-0.556	0.125
0.7000	-0.357	0.127	-0.374	0.133	-0.394	0.140	-0.416	0.148	-0.442	0.157
0.8000	-0.260	0.152	-0.272	0.159	-0.288	0.168	-0.303	0.177	-0.321	0.188
0.9000	-0.117	0.177	-0.123	0.185	-0.129	0.196	-0.136	0.208	-0.145	0.219
0.9500	0.005	0.215	0.005	0.225	0.006	0.238	0.006	0.251	0.006	0.266
1.0000	---	---	---	---	---	---	---	---	---	---

TABLE V

CALCULATION OF COMPRESSIBLE PRESSURE DISTRIBUTION FOR NACA 4412 AIRFOIL AT $C_l = 0.461$ USING KARMAN-TSIEN METHOD.

$$C_{p_m} = \frac{C_{p_i}}{\beta + k\, C_{p_i}} \text{ ; where } k = \frac{M^2}{2\left[\sqrt{1 - M^2} + 1\right]}$$

$\frac{x}{C}$	Incompressible		$M = 0.299$					
			$k = 0.023$			$\beta = 0.955$		
1	2	3	4	5	6	7	8	9
	$C_{p_{u_i}}$	$C_{p_{l_i}}$	$k\, C_{p_{u_i}}$	$k\, C_{p_{l_i}}$	$\beta + (4)$	$\beta + (5)$	$C_{p_{u_m}}$	$C_{p_{l_m}}$
0.0000	--	--	--	--	--	--	--	--
0.0125	0.220	-0.191	0.005	-0.004	0.960	0.951	0.229	-0.201
0.0250	-0.120	-0.300	-0.003	-0.007	0.952	0.948	-0.126	-0.316
0.0500	-0.315	-0.390	-0.007	-0.009	0.948	0.946	-0.332	-0.412
0.0750	-0.515	-0.280	-0.012	-0.006	0.943	0.949	-0.546	-0.295
0.1000	-0.580	-0.240	-0.014	-0.005	0.941	0.950	-0.616	-0.253
0.1500	-0.675	-0.167	-0.016	-0.004	0.939	0.951	-0.719	-0.176
0.2000	-0.710	-0.100	-0.016	-0.002	0.939	0.953	-0.756	-0.105
0.2500	-0.720	-0.048	-0.017	-0.001	0.938	0.954	-0.769	-0.050
0.3000	-0.710	-0.008	-0.016	0.000	0.939	0.955	-0.756	-0.008
0.4000	-0.645	0.049	-0.015	0.001	0.940	0.956	-0.686	0.051
0.5000	-0.540	0.069	-0.012	0.002	0.943	0.957	-0.572	0.072
0.6000	-0.450	0.101	-0.010	0.002	0.945	0.957	-0.476	0.106
0.7000	-0.357	0.127	-0.008	0.003	0.947	0.958	-0.377	0.132
0.8000	-0.260	0.152	-0.006	0.004	0.949	0.959	-0.274	0.158
0.9000	-0.117	0.177	-0.003	0.004	0.952	0.959	-0.123	0.185
0.9500	0.005	0.215	0.000	0.005	0.955	0.960	0.005	0.224
1.0000	--	--	--	--	--	--	--	--

TABLE V (Cont'd)

$\frac{x}{C}$	Incompressible		M = 0.427					
			k = 0.048			β = 0.905		
1	2	3	4	5	6	7	8	9
	$C_{p_{u_i}}$	$C_{p_{l_i}}$	$k\,C_{p_{u_i}}$	$k\,C_{p_{l_i}}$	$\beta+(4)$	$\beta+(5)$	$C_{p_{u_m}}$	$C_{p_{l_m}}$
0.0000	--	--	--	--	--	--	--	--
0.0125	0.220	-0.191	0.011	-0.009	0.916	0.896	0.240	-0.213
0.0250	-0.120	-0.300	-0.006	-0.014	0.899	0.891	-0.134	-0.337
0.0500	-0.315	-0.390	-0.015	-0.019	0.890	0.886	-0.352	-0.440
0.0750	-0.515	-0.280	-0.025	-0.013	0.880	0.892	-0.585	-0.314
0.1000	-0.580	-0.240	-0.030	-0.010	0.875	0.895	-0.662	-0.268
0.1500	-0.675	-0.167	-0.032	-0.008	0.873	0.897	-0.774	-0.186
0.2000	-0.710	-0.100	-0.034	-0.005	0.871	0.900	-0.815	-0.111
0.2500	-0.720	-0.048	-0.035	-0.002	0.870	0.903	-0.828	-0.054
0.3000	-0.710	-0.008	-0.034	0.000	0.871	0.905	-0.815	-0.009
0.4000	-0.645	0.049	-0.031	0.002	0.874	0.907	-0.739	0.054
0.5000	-0.540	0.069	-0.026	0.003	0.879	0.908	-0.615	0.076
0.6000	-0.450	0.101	-0.022	0.005	0.883	0.910	-0.510	0.111
0.7000	-0.357	0.127	-0.017	0.006	0.888	0.911	-0.402	0.139
0.8000	-0.260	0.152	-0.012	0.007	0.893	0.912	-0.291	0.167
0.9000	-0.117	0.177	-0.006	0.009	0.899	0.914	-0.130	0.194
0.9500	0.005	0.215	0.000	0.010	0.905	0.915	0.006	0.235
1.0000	--	--	--	--	--	--	--	--

TABLE V (Cont'd)

$\frac{x}{C}$	Incompressible		M = 0.517					
			k = 0.071			β = 0.858		
1	2	3	4	5	6	7	8	9
	$C_{p_{u_i}}$	$C_{p_{\ell_i}}$	$k\,C_{p_{u_i}}$	$k\,C_{p_{\ell_i}}$	β+(4)	β+(5)	$C_{p_{u_m}}$	$C_{p_{\ell_m}}$
0.0000	--	--	--	--	--	--	--	--
0.0125	0.220	-0.191	0.016	-0.014	0.874	0.844	0.252	-0.216
0.0250	-0.120	-0.300	-0.009	-0.021	0.849	0.837	-0.141	-0.358
0.0500	-0.315	-0.390	-0.022	-0.028	0.836	0.830	-0.377	-0.470
0.0750	-0.515	-0.280	-0.037	-0.020	0.821	0.838	-0.627	-0.334
0.1000	-0.580	-0.240	-0.044	-0.017	0.814	0.841	-0.714	-0.286
0.1500	-0.675	-0.167	-0.048	-0.012	0.810	0.846	-0.834	-0.197
0.2000	-0.710	-0.100	-0.050	-0.007	0.808	0.851	-0.879	-0.118
0.2500	-0.720	-0.048	-0.051	-0.003	0.807	0.855	-0.892	-0.056
0.3000	-0.710	-0.008	-0.050	-0.001	0.808	0.857	-0.879	-0.009
0.4000	-0.645	0.049	-0.046	0.003	0.812	0.861	-0.795	0.057
0.5000	-0.540	0.069	-0.038	0.005	0.820	0.863	-0.659	0.080
0.6000	-0.450	0.101	-0.032	0.007	0.826	0.865	-0.545	0.117
0.7000	-0.357	0.127	-0.025	0.009	0.833	0.867	-0.429	0.147
0.8000	-0.260	0.152	-0.018	0.011	0.840	0.869	-0.310	0.175
0.9000	-0.117	0.177	-0.008	0.013	0.850	0.871	-0.138	0.203
0.9500	0.005	0.215	0.000	0.015	0.858	0.873	0.006	0.246
1.0000	--	--	--	--	--	--	--	--

TABLE V (Cont'd)

$\frac{x}{C}$	Incompress-ible		M = 0.590					
			k = 0.096			β = 0.809		
1	2	3	4	5	6	7	8	9
	$C_{p_{u_i}}$	$C_{p_{\ell_i}}$	$k\,C_{p_{u_i}}$	$k\,C_{p_{\ell_i}}$	β+(4)	β+(5)	$C_{p_{u_m}}$	$C_{p_{\ell_m}}$
0.0000	--	--	--	--	--	--	--	--
0.0125	0.220	-0.191	0.021	-0.018	0.830	0.791	0.265	-0.242
0.0250	-0.120	-0.300	-0.012	-0.029	0.797	0.780	-0.151	-0.384
0.0500	-0.315	-0.390	-0.030	-0.037	0.779	0.772	-0.405	-0.505
0.0750	-0.515	-0.280	-0.049	-0.027	0.760	0.782	-0.679	-0.358
0.1000	-0.580	-0.240	-0.056	-0.023	0.753	0.786	-0.770	-0.306
0.1500	-0.675	-0.167	-0.065	-0.016	0.744	0.793	-0.908	-0.211
0.2000	-0.710	-0.100	-0.068	-0.010	0.741	0.799	-0.960	-0.125
0.2500	-0.720	-0.048	-0.069	-0.005	0.740	0.804	-0.974	-0.060
0.3000	-0.710	-0.008	-0.068	-0.001	0.741	0.808	-0.960	-0.010
0.4000	-0.645	0.049	-0.062	0.005	0.747	0.814	-0.864	0.060
0.5000	-0.540	0.069	-0.052	0.007	0.757	0.816	-0.714	0.085
0.6000	-0.450	0.101	-0.043	0.010	0.766	0.819	-0.587	0.124
0.7000	-0.357	0.127	-0.034	0.012	0.775	0.821	-0.461	0.155
0.8000	-0.260	0.152	-0.025	0.015	0.784	0.824	-0.332	0.185
0.9000	-0.117	0.177	-0.011	0.017	0.798	0.826	-0.147	0.214
0.9500	0.005	0.215	0.000	0.021	0.809	0.830	0.006	0.259
1.0000	--	--	--	--	--	--	--	--

TABLE VI

EXPERIMENTAL DATA FOR NACA 4412 AIRFOIL AT $\alpha = -0.25°$.
(8, p.78)

	M = 0.299		M = 0.427		M = 0.517		M = 0.590	
$\frac{x}{C}$	$C_{p_{u_m}}$	$C_{p_{\ell_m}}$	$C_{p_{u_m}}$	$C_{p_{\ell_m}}$	$C_{p_{u_m}}$	$C_{p_{\ell_m}}$	$C_{p_{u_m}}$	$C_{p_{\ell_m}}$
0.0000	1.00	1.00	1.00	1.00	1.00	1.00	1.00	1.00
0.0125	0.05	0.02	0.20	-0.05	0.30	-0.05	0.40	-0.15
0.0250	-0.20	-0.30	-0.18	-0.40	-0.10	-0.41	-0.10	-0.40
0.0500	-0.38	-0.34	-0.35	-0.42	-0.38	-0.45	-0.38	-0.50
0.0750	-0.52	-0.30	-0.50	-0.37	-0.54	-0.40	-0.55	-0.42
0.1000	-0.60	-0.26	-0.62	-0.30	-0.66	-0.33	-0.72	-0.38
0.1500	-0.70	-0.18	-0.73	-0.21	-0.80	-0.22	-0.90	-0.26
0.2000	-0.77	-0.10	-0.80	-0.14	-0.90	-0.14	-1.02	-0.15
0.2500	-0.80	-0.02	-0.84	-0.06	-0.94	-0.08	-1.10	-0.10
0.3000	-0.78	0.00	-0.84	-0.02	-0.94	-0.05	-1.08	-0.08
0.4000	-0.70	0.03	-0.74	0.02	-0.85	0.00	-0.94	0.00
0.5000	-0.60	0.06	-0.62	0.05	-0.70	0.05	-0.78	0.04
0.6000	-0.46	0.09	-0.49	0.07	-0.55	0.07	-0.62	0.06
0.7000	-0.37	0.10	-0.40	0.10	-0.44	0.09	-0.48	0.07
0.8000	-0.25	0.11	-0.25	0.12	-0.28	0.12	-0.31	0.08
0.9000	-0.08	0.14	-0.075	0.14	-0.08	0.15	-0.10	0.10
0.9500	0.05	0.16	0.06	0.15	0.06	0.16	0.02	0.15
1.0000	0.17	0.17	0.16	0.16	0.17	0.17	0.15	0.15

TABLE VII

CALCULATION OF EXPERIMENTAL PRESSURE DISTRIBUTION AT $\alpha = 1.88°$.

(Correction of Experimental C_{p_m} at M = 0.141 to C_{p_i} at M = 0).

(By the Relation [Prandtl-Glauert], $C_{p_i} = \beta C_{p_m}$; $\beta = 0.983$).

$\frac{x}{C}$	# M = 0.191		M = 0	
	C_{p_u}	C_{p_l}	C_{p_u}	C_{p_l}
0.0000	0.60	1.000	0.590	0.983
0.0125	-0.52	0.600	-0.511	0.590
0.0250	-0.70	0.330	-0.689	0.324
0.0500	-0.80	0.040	-0.787	0.039
0.0750	-0.87	0.015	-0.855	0.0147
0.1000	-0.92	0.000	-0.915	0.000
0.1500	-0.96	0.015	-0.944	0.0147
0.2000	-0.99	0.050	-0.974	0.049
0.2500	-0.97	0.075	-0.954	0.074
0.3000	-0.95	0.090	-0.934	0.089
0.4000	-0.84	0.110	-0.826	0.108
0.5000	-0.65	0.120	-0.639	0.118
0.6000	-0.54	0.135	-0.531	0.133
0.7000	-0.40	0.150	-0.393	0.147
0.8000	-0.26	0.155	-0.255	0.152
0.9000	-0.09	0.160	-0.089	0.157
0.9500	0.05	0.160	0.049	0.157
1.0000	0.15	0.150	0.147	0.147

Data from (8, p.80)

TABLE VIII

VELOCITY DISTRIBUTION CALCULATION FOR NACA 4412 AIRFOIL AT $C_l = 0.687$ ($\alpha = 1.88°$).
(Incompressible Flow)

$$\eta = (C_l - C_{l_b}) = (0.687 - 0.587) = 0.10$$

$\frac{x}{C}$	# P_b ($C_{l_b} = 0.587$)	# $\frac{P_a}{C_{l_a}}$	$\frac{P_a}{C_{l_a}}(\eta)$	P ($C = 0.687$)	$\frac{w_f}{U}$	$P/4/w_f/U$	$\frac{w_u}{U}$	$\frac{w_l}{U}$
0.0000	0.0000	0.000	0.000	0.000	0.000	---	---	---
0.0125	0.2710	5.408	0.541	0.812	0.987	0.2055	1.1925	0.7815
0.0250	0.3550	4.235	0.424	0.779	1.099	0.1773	1.2763	0.9217
0.0500	0.4720	3.126	0.313	0.785	1.163	0.1688	1.3318	0.9942
0.0750	0.5540	2.560	0.256	0.810	1.181	0.1713	1.3523	1.0097
0.1000	0.6200	2.199	0.220	0.840	1.188	0.1769	1.3649	1.0111
0.1500	0.7240	1.742	0.174	0.898	1.187	0.1891	1.3761	0.9979
0.2000	0.7920	1.454	0.145	0.937	1.179	0.1989	1.3779	0.9801
0.2500	0.8280	1.248	0.125	0.953	1.168	0.2040	1.3720	0.9640
0.3000	0.8410	1.090	0.109	0.950	1.156	0.2055	1.3615	0.9505
0.4000	0.8020	0.854	0.085	0.887	1.129	0.1967	1.3257	0.9323
0.5000	0.6940	0.681	0.068	0.762	1.103	0.1728	1.2758	0.9302
0.6000	0.6220	0.542	0.054	0.676	1.076	0.1572	1.2332	0.9188
0.7000	0.5430	0.424	0.042	0.585	1.050	0.1393	1.1893	0.9107
0.8000	0.4510	0.315	0.032	0.483	1.022	0.1180	1.1400	0.9040
0.9000	0.3200	0.202	0.020	0.340	0.982	0.0865	1.0685	0.8955
0.9500	0.2270	0.134	0.013	0.240	0.942	0.0637	1.0057	0.8783
1.0000	0.0000	0.000	0.000	0.000	0.000	---	---	---

#Data from (1, p.23)

TABLE IX

CALCULATION OF INCOMPRESSIBLE PRESSURE DISTRIBUTION FOR NACA 4412 AIRFOIL AT $C_\ell = 0.687$ ($\alpha = 1.88°$).

$\frac{x}{c}$	$(\frac{w_u}{U})^2$	$(\frac{w_\ell}{U})^2$	$C_{p_{u_i}} = 1-(\frac{w_u}{U})^2$	$C_{p_{\ell_i}} = 1-(\frac{w_\ell}{U})^2$
0.0000	---	---	---	---
0.0125	1.420	0.611	-0.420	0.389
0.0250	1.625	0.850	-0.625	0.150
0.0500	1.750	0.988	-0.750	0.012
0.0750	1.830	1.019	-0.830	-0.019
0.1000	1.865	1.022	-0.865	-0.022
0.1500	1.894	0.996	-0.894	0.004
0.2000	1.900	0.961	-0.900	0.039
0.2500	1.882	0.930	-0.882	0.070
0.3000	1.855	0.904	-0.855	0.096
0.4000	1.758	0.870	-0.758	0.130
0.5000	1.628	0.867	-0.628	0.133
0.6000	1.522	0.843	-0.522	0.157
0.7000	1.415	0.830	-0.415	0.170
0.8000	1.300	0.818	-0.300	0.182
0.9000	1.142	0.802	-0.142	0.198
0.9500	1.012	0.772	-0.012	0.228
1.0000	---	---	---	---

TABLE X

CALCULATION OF COMPRESSIBLE PRESSURE DISTRIBUTION FOR NACA 4412 AIRFOIL AT $\alpha = 1.88°$ USING PRANDTL-GLAUERT METHOD.

$$C_{p_m} = \frac{C_{p_i}}{\beta}$$

$\frac{x}{c}$	Incompressible		M = 0.512		M = 0.596		M = 0.640		M = 0.735	
			β = 0.859		β = 0.804		β = 0.770		β = 0.678	
	C_{p_u}	C_{p_l}	C_{p_u}	C_{p_l}	C_{p_u}	C_{p_l}	C_{p_u}	C_{p_l}	C_{p_u}	C_{p_l}
0.0000	---	---	---	---	---	---	---	---	---	---
0.0125	-0.420	0.389	-0.489	0.452	-0.523	0.484	-0.546	0.505	-0.620	0.574
0.0250	-0.625	0.150	-0.728	0.175	-0.777	0.187	-0.812	0.195	-0.922	0.221
0.0500	-0.750	0.012	-0.874	0.014	-0.934	0.015	-0.975	0.0156	-1.107	0.0177
0.0750	-0.830	-0.019	-0.966	-0.022	-1.031	-0.024	-1.080	-0.025	-1.250	-0.028
0.1000	-0.865	-0.022	-1.007	-0.026	-1.075	-0.027	-1.125	-0.029	-1.280	-0.0325
0.1500	-0.894	0.004	-1.042	0.005	-1.112	0.005	-1.161	0.0052	-1.320	0.006
0.2000	-0.900	0.039	-1.047	0.045	-1.120	0.048	-1.170	0.051	-1.330	0.058
0.2500	-0.882	0.070	-1.037	0.082	-1.098	0.087	-1.147	0.091	-1.302	0.103
0.3000	-0.855	0.096	-0.995	0.112	-1.063	0.119	-1.110	0.125	-1.260	0.142
0.4000	-0.758	0.130	-0.883	0.151	-0.943	0.162	-0.985	0.169	-1.120	0.192
0.5000	-0.628	0.133	-0.731	0.155	-0.781	0.165	-0.816	0.173	-0.927	0.196
0.6000	-0.522	0.157	-0.607	0.183	-0.649	0.195	-0.678	0.204	-0.771	0.232
0.7000	-0.415	0.170	-0.483	0.198	-0.516	0.211	-0.539	0.221	-0.612	0.251
0.8000	-0.300	0.182	-0.349	0.212	-0.373	0.227	-0.390	0.236	-0.443	0.269
0.9000	-0.142	0.198	-0.165	0.231	-0.177	0.246	-0.185	0.257	-0.210	0.292
0.9500	-0.012	0.228	-0.014	0.266	-0.015	0.284	-0.0156	0.296	-0.0177	0.336
1.0000	---	---	---	---	---	---	---	---	---	---

TABLE XI

CALCULATION OF COMPRESSIBLE PRESSURE DISTRIBUTION FOR NACA 4412 AIRFOIL AT $\alpha = 1.88°$ USING KARMAN-TSIEN METHOD.

$$C_{p_m} = \frac{C_{p_i}}{\beta + k\, C_{p_i}} \text{ ; where } k = \frac{M^2}{2\left[\sqrt{1 - M^2} + 1\right]}$$

$\frac{x}{C}$	Incompressible		M = 0.512					
			k = 0.0708				β = 0.859	
1	2	3	4	5	6	7	8	9
	$C_{p_{u_i}}$	$C_{p_{\ell_i}}$	$k\, C_{p_{u_i}}$	$k\, C_{p_{\ell_i}}$	β+(4)	β+(5)	$C_{p_{u_m}}$	$C_{p_{\ell_m}}$
0.0000	--	--	--	--	--	--	--	--
0.0125	-0.420	0.389	-0.030	0.028	0.829	0.887	-0.507	0.439
0.0250	-0.625	0.150	-0.044	0.011	0.815	0.870	-0.767	0.172
0.0500	-0.750	0.012	-0.053	0.001	0.806	0.860	-0.931	0.014
0.0750	-0.830	-0.019	-0.059	-0.001	0.800	0.858	-1.039	-0.022
0.1000	-0.865	-0.022	-0.061	-0.001	0.798	0.858	-1.083	-0.026
0.1500	-0.894	0.004	-0.063	0.000	0.796	0.859	-1.122	0.005
0.2000	-0.900	0.039	-0.064	0.003	0.795	0.862	-1.132	0.045
0.2500	-0.882	0.070	-0.063	0.005	0.796	0.864	-1.110	0.081
0.3000	-0.855	0.096	-0.061	0.007	0.798	0.866	-1.071	0.111
0.4000	-0.758	0.130	-0.054	0.009	0.805	0.868	-0.943	0.150
0.5000	-0.628	0.133	-0.044	0.009	0.815	0.868	-0.771	0.153
0.6000	-0.522	0.157	-0.037	0.011	0.822	0.870	-0.635	0.181
0.7000	-0.415	0.170	-0.029	0.012	0.830	0.871	-0.500	0.195
0.8000	-0.300	0.182	-0.021	0.013	0.838	0.872	-0.358	0.209
0.9000	-0.142	0.198	-0.010	0.014	0.849	0.873	-0.157	0.227
0.9500	-0.012	0.228	-0.001	0.016	0.858	0.875	-0.014	0.261
1.0000	--	--	--	--	--	--	--	--

TABLE XI (Cont'd)

$\frac{x}{C}$	Incompress-ible		M = 0.596					
			k = 0.098				β = 0.804	
1	2	3	4	5	6	7	8	9
	$C_{p_{u_i}}$	$C_{p_{l_i}}$	$k\,C_{p_{u_i}}$	$k\,C_{p_{l_i}}$	β+(4)	β+(5)	$C_{p_{u_m}}$	$C_{p_{l_m}}$
0	--	--	--	--	--	--	--	--
0.0125	-0.420	0.389	-0.041	0.038	0.763	0.842	-0.550	0.462
0.0250	-0.625	0.150	-0.061	0.015	0.743	0.819	-0.841	0.183
0.0500	-0.750	0.012	-0.074	0.001	0.730	0.805	-1.027	0.015
0.0750	-0.830	-0.019	-0.081	-0.002	0.723	0.806	-1.148	-0.023
0.1000	-0.865	-0.022	-0.085	-0.002	0.719	0.802	-1.203	-0.027
0.1500	-0.894	0.004	-0.088	0.000	0.716	0.804	-1.250	0.005
0.2000	-0.900	0.039	-0.088	0.004	0.716	0.808	-1.257	0.048
0.2500	-0.882	0.070	-0.087	0.007	0.717	0.811	-1.230	0.086
0.3000	-0.855	0.096	-0.084	0.009	0.720	0.813	-1.188	0.118
0.4000	-0.758	0.130	-0.074	0.013	0.730	0.817	-1.040	0.159
0.5000	-0.628	0.133	-0.062	0.013	0.742	0.817	-0.847	0.163
0.6000	-0.522	0.157	-0.051	0.015	0.753	0.819	-0.693	0.192
0.7000	-0.415	0.170	-0.040	0.017	0.764	0.821	-0.543	0.207
0.8000	-0.300	0.182	-0.030	0.018	0.774	0.822	-0.389	0.221
0.9000	-0.142	0.198	-0.014	0.019	0.790	0.823	-0.180	0.241
0.9500	-0.012	0.228	-0.001	0.022	0.803	0.826	-0.015	0.276
1.0000	--	--	--	--	--	--	--	--

TABLE XI (Cont'd)

$\frac{x}{c}$	Incompressible		M = 0.640					
			k = 0.116				β = 0.770	
1	2	3	4	5	6	7	8	9
	$C_{p_{u_i}}$	$C_{p_{\ell_i}}$	$k\,C_{p_{u_i}}$	$k\,C_{p_{\ell_i}}$	$\beta+(4)$	$\beta+(5)$	$C_{p_{u_m}}$	$C_{p_{\ell_m}}$
0	--	--	--	--	--	--	--	--
0.0125	-0.420	0.389	-0.049	0.045	0.721	0.815	-0.583	0.477
0.0250	-0.625	0.150	-0.073	0.017	0.697	0.787	-0.896	0.191
0.0500	-0.750	0.012	-0.087	0.001	0.683	0.771	-1.099	0.016
0.0750	-0.830	-0.019	-0.096	-0.002	0.674	0.768	-1.233	-0.025
0.1000	-0.865	-0.022	-0.100	-0.003	0.670	0.767	-1.290	-0.029
0.1500	-0.894	0.004	-0.104	0.000	0.666	0.770	-1.342	0.005
0.2000	-0.900	0.039	-0.104	0.005	0.666	0.775	-1.350	0.050
0.2500	-0.882	0.070	-0.102	0.008	0.668	0.778	-1.323	0.090
0.3000	-0.855	0.096	-0.099	0.011	0.671	0.781	-1.275	0.123
0.4000	-0.758	0.130	-0.088	0.015	0.682	0.785	-1.112	0.166
0.5000	-0.628	0.133	-0.073	0.015	0.697	0.785	-0.900	0.170
0.6000	-0.522	0.157	-0.061	0.018	0.709	0.788	-0.736	0.199
0.7000	-0.415	0.170	-0.048	0.020	0.722	0.790	-0.575	0.215
0.8000	-0.300	0.182	-0.035	0.021	0.735	0.791	-0.408	0.230
0.9000	-0.142	0.198	-0.016	0.023	0.754	0.793	-0.188	0.250
0.9500	-0.012	0.228	-0.001	0.026	0.769	0.796	-0.016	0.287
1.0000	--	--	--	--	--	--	--	--

TABLE XI (Cont'd)

$\frac{x}{C}$	Incompressible		M = 0.735					
			k = 0.161				β = 0.678	
1	2	3	4	5	6	7	8	9
	$C_{p_{u_i}}$	$C_{p_{\ell_i}}$	$k\,C_{p_{u_i}}$	$k\,C_{p_{\ell_i}}$	β +(4)	β +(5)	$C_{p_{u_m}}$	$C_{p_{\ell_m}}$
0	--	--	--	--	--	--	--	--
0.0125	-0.420	0.389	-0.068	0.063	0.610	0.741	-0.688	0.525
0.0250	-0.625	0.150	-0.100	0.024	0.578	0.702	-1.081	0.208
0.0500	-0.750	0.012	-0.121	0.002	0.557	0.680	-1.345	0.018
0.0750	-0.830	-0.019	-0.134	-0.003	0.544	0.675	-1.525	-0.028
0.1000	-0.865	-0.022	-0.139	-0.004	0.539	0.674	-1.605	-0.033
0.1500	-0.894	0.004	-0.144	0.001	0.534	0.679	-1.675	0.006
0.2000	-0.900	0.039	-0.145	0.006	0.533	0.684	-1.688	0.057
0.2500	-0.882	0.070	-0.142	0.011	0.536	0.689	-1.645	0.102
0.3000	-0.855	0.096	-0.138	0.015	0.540	0.694	-1.582	0.138
0.4000	-0.758	0.130	-0.122	0.021	0.556	0.699	-1.363	0.186
0.5000	-0.628	0.133	-0.101	0.021	0.577	0.699	-1.089	0.190
0.6000	-0.522	0.157	-0.084	0.025	0.594	0.703	-0.879	0.224
0.7000	-0.415	0.170	-0.067	0.027	0.611	0.705	-0.680	0.241
0.8000	-0.300	0.182	-0.048	0.029	0.630	0.707	-0.476	0.257
0.9000	-0.142	0.198	-0.023	0.032	0.655	0.710	-0.217	0.279
0.9500	-0.012	0.228	-0.002	0.036	0.676	0.714	-0.018	0.320
1.0000	--	--	--	--	--	--	--	--

TABLE XII

EXPERIMENTAL DATA FOR NACA 4412 AIRFOIL AT $\alpha = 1.88°$.
(8, p.80)

	M = 0.512		M = 0.596		M = 0.640		M = 0.735	
$\frac{x}{c}$	----		$C_{p_c} = -1.33$		$C_{p_c} = -1.08$		$C_{p_c} = -0.64$	
	C_{p_u}	C_{p_l}	C_{p_u}	C_{p_l}	C_{p_u}	C_{p_l}	C_{p_u}	C_{p_l}
0.0000	1.08	0.90	1.05	1.00	1.10	0.88	1.10	-0.044
0.0125	0.20	0.55	-0.30	0.40	-0.10	0.17	0.60	-0.10
0.0250	-0.40	0.08	-0.65	0.06	-0.40	-0.03	0.20	-0.50
0.0500	-0.825	-0.04	-0.80	-0.10	-0.68	-0.14	-0.15	-0.73
0.0750	-0.95	-0.07	-0.97	-0.12	-0.87	-0.15	-0.34	-0.68
0.1000	-1.04	-0.06	-1.08	-0.10	-1.02	-0.13	-0.52	-0.60
0.1500	-1.13	-0.02	-1.27	-0.06	-1.25	-0.08	-0.73	-0.45
0.2000	-1.19	0.01	-1.38	-0.02	-1.39	-0.04	-0.92	-0.27
0.2500	-1.19	0.05	-1.42	0.02	-1.49	0.01	-1.00	-0.21
0.3000	-1.14	0.08	-1.38	0.05	-1.54	0.05	-1.05	-0.16
0.4000	-0.98	0.10	-1.13	0.08	-1.53	0.08	-1.22	-0.11
0.5000	-0.76	0.10	-0.85	0.11	-0.83	0.08	-1.38	-0.08
0.6000	-0.62	0.125	-0.67	0.12	-0.70	0.11	-1.32	-0.07
0.7000	-0.45	0.17	-0.48	0.13	-0.52	0.12	-0.092	-0.05
0.8000	-0.28	0.17	-0.30	0.14	-0.30	0.13	-0.50	-0.03
0.9000	-0.07	0.16	-0.07	0.14	-0.07	0.13	-0.25	-0.04
0.9500	0.06	0.15	0.05	0.12	0.05	0.11	-0.18	-0.05
1.0000	0.13	0.13	0.10	0.10	0.10	0.10	-0.08	-0.08

TABLE XIII

CALCULATION OF C_ℓ VALUES FROM PRESSURE DISTRIBUTION CURVES.

$\alpha = -0.25°$, $\cos\alpha = 0.99999$

M	Prandtl-Glauert			Karman-Tsien			Experimental		
	$A(in.^2)$	C_n	$C_\ell = C_n \cos\alpha$	A	C_n	C_ℓ	A	C_n	C_ℓ
0.299	6.00	0.480	0.480	6.16	0.493	0.493	5.94	0.475	0.475
0.427	6.46	0.516	0.515	6.64	0.531	0.530	6.04	0.483	0.483
0.517	6.82	0.546	0.545	6.88	0.551	0.550	6.50	0.520	0.519
0.590	7.11	0.569	0.568	7.54	0.603	0.602	7.15	0.571	0.570

$\alpha = 1.88°$, $\cos\alpha = 0.99947$

M	A	C_n	C_ℓ	A	C_n	C_ℓ	A	C_n	C_ℓ
0.512	9.75	0.780	0.779	10.42	0.834	0.833	9.75	0.780	0.779
0.596	10.60	0.847	0.846	11.36	0.908	0.906	10.45	0.836	0.835
0.640	11.10	0.888	0.887	12.08	0.966	0.964	10.88	0.870	0.869
0.735	12.68	1.014	1.012	14.55	1.162	1.160	9.68	0.774	0.773